(NASA-CR-176615) EXPLORATORY LOW-SPEED WIND-TUNNEL STUDY OF CONCEPTS DESIGNED TO IMPROVE AIRCRAFT STABILITY AND CONTROL AT HIGH ANGLES OF ATTACK M.S. Thesis (George Washington Univ.) 73 p HC A04/MF A01 G3/02

N86-20344

Unclas 00634

EXPLORATORY LOW-SPEED WIND-TUNNEL STUDY OF CONCEPTS DESIGNED TO IMPROVE AIRCRAFT STABILITY AND CONTROL AT HIGH ANGLES OF ATTACK

By

David Edgar Hahne

B.S June 1981, Virginia Polytechnic Institute and State University

A Thesis submitted to the Faculty of

The Gradueate School of Engineering and Applied Science of

The George Washington University

in partial satisfaction of the requirements for

the degree of Master of Science

December 1985

ABSTRACT

A wind-tunnel investigation of concepts to improve the high angle-of-attack stability and control characteristics of a high performance aircraft has been conducted. The effect of vertical tail geometry on stability and the effectiveness of several conventional and unusual control concepts has been determined. These results were obtained over a large angle-of-attack range. It was found that vertical tail location, cant angle and leading edge sweep could influence both longitudinal and lateral-directional stability. The control concepts tested were found to be effective and to provide control into the post-stall angle-of-attack region.

ACKNOWLEDGEMENTS

The author wishes to thank the National Aeronautics and Space Administration for providing the opportunity to perform this research, prepare this thesis, and complete all the other requirements for this degree. The author is grateful to Professor John P. Campbell who acted as academic and thesis advisor. His guidance and encouragement have been instrumental in the successful completion of my degree program. I would also like to thank Mr. Joseph L. Johnson for his guidance throughout this test program, Ms Jennifer D. Irby for her speedy preparation of this document and Mr. Stanley H. Husch for his exceptional work in preparing the figures contained herein. Special thanks also go to Mr. Mark A. Croom and Mr. Luat T. Nguyen for their helpful insights in analyzing and interpreting the results presented in this thesis.

TABLE OF CONTENTS

LIST OF TABLES

LIST OF FIGURES

LIST OF SYMBOLS

	aspect ratio
b	wing span, ft
C_L	lift coefficient, Lift/$\bar{q}S$
C_ℓ	rolling-moment coefficient, Rolling moment/$\bar{q}Sb$
C_m	pitching-moment coefficient, Pitching moment/$\bar{q}S\bar{c}$
C_n	yawing-moment coefficient, Yawing moment/$\bar{q}Sb$
C_Y	side-force coefficient, Side force/$\bar{q}S$
$\bar{c}$	mean aerodynamic chord, ft
I_x, I_y, I_z	mass moments of inertia about X_b, Y_b, Z_b body axes, slugs-ft^2
M	mach number
m	aircraft mass, slugs
p, q, r	angular velocity about the X_b, Y_b, and Z_b body axes, deg/sec
p_s	roll rate about the velocity vector, deg/sec
$\dot{p}$, $\dot{q}$, $\dot{r}$	angular acceleration about the X_b, Y_b, and Z_b body axes, deg/sec^2
$\bar{q}$	freestream dynamic pressure, lbs/ft^2
S	wing area, ft^2
s	Laplace transform variable
u, v, w	linear velocities along the X_b, Y_b, Z_b body axes, ft/sec
V	freestream velocity, ft/sec
X_b, Y_b, Z_b	body axes
y	span ordinate, ft
$2y/b$	nondimensional semispan location
α	angle of attack, deg
β	angle of sideslip, deg

ΔC_ℓ	incremental rolling moment coefficient
ΔC_n	incremental yawing moment coefficient
ΔC_Y	incremental side force coefficient
δ_a	aileron deflection, deg
δ_{CL}	centerline vertical tail deflection, deg
δ_c	canard deflection, deg
δ_F	trailing edge extension flap deflection, deg
δ_f	leading edge flap deflection, deg
δ_h	horizontal tail deflection, deg
δ_r	rudder deflection, deg
δ_{ra}	aft swept tail rudder deflection, deg
δ_{rf}	forward swept tail rudder deflection, deg
δ_{rt}	tip rudder deflection, deg
δ_{wt}	wing tip deflection, deg
λ	root of characteristic equation
φ	aircraft roll attitude, deg
ρ	air density, slugs/ft^3

Stability derivatives

$$C_{\ell_p} = \frac{\partial C_\ell}{\frac{\partial pb}{2V}} \qquad C_{\ell_r} = \frac{\partial C_\ell}{\frac{\partial rb}{2V}} \qquad C_{\ell_\beta} = \frac{\partial C_\ell}{\partial \beta} \qquad C_{\ell_{\delta a}} = \frac{\partial C_\ell}{\partial \delta_a} \qquad C_{\ell_{\delta r}} = \frac{\partial C_\ell}{\partial \delta_r}$$

$$C_{m_{\delta e}} = \frac{\partial C_m}{\partial \delta_e} \qquad C_{n_p} = \frac{\partial C_n}{\frac{\partial pb}{2V}} \qquad C_{n_r} = \frac{\partial C_n}{\frac{\partial rb}{2V}} \qquad C_{n_\beta} = \frac{\partial C_n}{\partial \beta} \qquad C_{n_{\delta a}} = \frac{\partial C_n}{\partial \delta_a}$$

$$C_{n_{\delta r}} = \frac{\partial C_n}{\partial \delta_r} \qquad C_Y = \frac{\partial C_Y}{\frac{\partial pb}{2V}} \qquad C_{Y_r} = \frac{\partial C_Y}{\frac{\partial rb}{2V}} \qquad C_Y = \frac{\partial C_Y}{\partial \beta}$$

Subscripts

IB	inboard
MB	midboard
OB	outboard

CHAPTER 1

INTRODUCTION

The emphasis on sustained nonafterburning supersonic cruise makes aircraft with high-fineness-ratio fuselages, low-aspect-ratio, highly-swept wings and highly-integrated control surfaces attractive because of low cruise drag (Reference 1). These same features, however, make the aircraft more susceptible to the development and sudden breakdown of strong vortical flowfields at angles of attack and speeds encountered during maneuvering. This is especially true above 15° angle of attack where the vortical flowfields can produce nonlinearities and regions of unstable behavior in the longitudinal, lateral and directional aerodynamics. In addition strong spanwise flowfields arise which reduce the effectiveness of conventional control devices. Such aerodynamic characteristics complicate control system design especially for unstable aircraft where powerful control surfaces are the key to a successful active flight control system.

As illustrated conceptually in figure 1, maneuverability decreases with increasing angle of attack such that very little capability is available at and above the stall. On some configurations, limiters are imposed to avoid susceptibility to loss of control and spins. Providing controls that maintain a high level of effectiveness will allow future high performance aircraft to exploit a much larger angle-of-attack envelope, including brief excursions into post stall flight conditions. A major potential payoff is configuration optimization flexibility which results from the fact that the high levels of control effectiveness combined with appropriate control laws and fly-by-wire technology will allow increased reliance on stability and control augmentation. This will allow the designer greater freedom in optimizing the configuration to meet other requirements such as minimum drag at cruise conditions (figure 2). Typically,

designs that have originally been optimized for supersonic cruise performance have had to be modified to obtain acceptable low-speed characteristics at the expense of cruise performance (Reference 2). Advanced controls technology can minimize this required compromise in future high performance aircraft.

As part of a NASA Langley Research Center Flight Dynamics Branch and McDonnell Aircraft Company cooperative research program, an investigation of advanced control concepts for high performance aircraft applications has been performed. The primary objectives were: (1) to develop aerodynamic control devices that maintain desired level of effectiveness throughout the maneuvering angle-of-attack range, including stall and post-stall conditions; and (2) to study the impact that these advances will have on aircraft maneuverability and the associated flight dynamics. The generic configuration of this study has emerged from a number of studies aimed at developing design guidelines for providing efficient supersonic cruise, transonic maneuvering capability comparable to current high performance aircraft and good low-speed/high angle-of-attack stability and control (Reference 3). This thesis presents the results of the latest phase of this group of studies to develop and evaluate conventional and unusual control concepts for advanced aircraft. This work includes an evaluation of the effects of tail geometry on stability as well as an evaluation of control effectiveness. Comparisons of maneuverability with a highly-maneuverable aircraft are also presented.

The test program was conducted in the Langley Research Center's 12-Foot Low-Speed Wind Tunnel using a strut supported scale model of the generic configuration. Data were taken over a large angle-of-attack range at several sideslip angles.

CHAPTER 2

MODEL AND APPARATUS

The basic model and its support system are shown in figure 3. Details of the model forebody, vertical tails, control surfaces, and horizontal tails and canards are shown in figures 4, 5, 6, and 7, respectively. The arrow wing had a 65° swept leading edge with an aspect ratio of 1.95. The wings, tails and canards all had thin flat-plate cross-sections (for simplicity) with beveled leading and trailing edges. The wing leading edge was divided into three flap segments and the trailing edge had two different flap/aileron configurations along with flaps on the inboard trailing edge extension. It was also possible to deflect the wing tips as ailerons. The trailing edge extension was removable and could be replaced by horizontal tails. The fuselage could also be adapted to use canards. The model could be configured with three different vertical tail arrangements: forward and aft swept twin tails (mounted on the trailing edge extensions) and a single centerline tail. The vertical tails also had several fore and aft positions as well as the ability to cant either inboard or outboard. The fuselage, with flow through ducts, was strut mounted to minimize unfavorable effects on vortex bursting as described in Reference 4.

Force and moment data were obtained using a six component strain-gage balance mounted inside the model fuselage. The voltage outputs of the strain-gage balance were converted to digital signals by a NEFF 620 amplifier/multiplexor. The NEFF 620 provided the required signal processing for use with the HP-9845B microcomputer used for data reduction and storage. The data acquisition system sampled each balance output 100 times over 10 seconds and averaged the data. Non-dimensional coefficients were then calculated and stored on magnetic discs.

CHAPTER 3

WIND TUNNEL TESTS

Static force tests were conducted in the Langley Research Center's 12-Foot Low Speed Wind Tunnel. A photograph of the model in the test section is presented in figure 8. The tests were conducted at a freestream dynamic pressure of 4 psf (M = .05) which corresponds to a Reynolds number of 0.62×10^6 based on wing mean aerodynamic chord. Data were obtained over an angle of attack range from 0° to 60° at angles of sideslip of 0° and ±5°. No corrections for base drag or wall effects were made to the data. Flow angularity corrections were made for both angle of attack and angle of sideslip.

In the first part of the test program, studies were made of the effect of spanwise location for the aft swept tails and tail cant (from 30° inboard to 30° outboard) for the forward and aft swept twin vertical tails. Once an optimum cant angle was obtained, rudder effectiveness was determined. An all moving centerline tail was also investigated. Various pitch control devices were examined including horizontal tails, canards, trailing edge extension flaps and ailerons deflected symmetrically. Two types of ailerons were investigated: unswept hingeline ailerons and constant chord ailerons. Deflected wing tips were also investigated for roll control.

All data were initially obtained about the body axes (figure 9). All lateral-directional data are presented about the body axes, but all the longitudinal data are presented about the stability axes.

CHAPTER 4

ANALYSIS TECHNIQUES

A calculated parameter which is useful for the analysis of high angle-of-attack lateral-directional stability is $C_{n_{\beta,dyn}}$ (Reference 5), defined as

$$C_{n_{\beta,dyn}} = C_{n_\beta} \cos \alpha - \frac{I_z}{I_x} C_{\ell_\beta} \sin \alpha \qquad (1)$$

Negative values of this parameter indicate a susceptibility to a divergence (nose slice). This term is derived from one of the coefficients of the lateral open-loop characteristic equation in which A, B, C, D and E are constants.

$$A\lambda^4 + B\lambda^3 + C\lambda^2 + D\lambda + E = 0 \qquad (1)$$

This equation will have unstable roots if any of the coefficients or Routh's discriminant ($BDC - AD^2 - B^2E$) becomes negative. In particular, if the C-coefficient becomes negative a directional divergence usually occurs. Neglecting the products of inertia the C-coefficient is given by:

$$C = \mu[-K_1 C_{y_r} C_{n_\beta} + K_1 C_{n_r} C_{y_\beta} + 4\mu K_1 C_{n_\beta} \cos \alpha + K_2 C_{\ell_p}$$
$$K_2 C_{\ell_\beta} C_{y_p} - 4\mu K_2 C_{\ell_p} \sin \alpha + 1/2 C_{n_r} C_{\ell_p} - 1/2 C_{n_p} C_{\ell_r}] \qquad (2)$$

where

$$\mu = \frac{m}{\rho S b}$$

$$K_1 = \frac{I_x}{m b^2}$$

and

$$K_2 = \frac{I_z}{m b^2}$$

Neglecting products of derivatives (which in general are <<1)

$$C = 4\mu^2 \left[K_1 C_{n_\beta} \cos \alpha - K_2 C_{\ell_\beta} \sin \alpha \right] \tag{3}$$

By removing the common terms and dividing equation 3 by A_X, equation 1 is obtained. Normally, this equation is reduced further by assuming $\cos \alpha = 1$, but for this study the cosine term was retained for exactness because of the large angles of attack involved. The work in Reference 6 has shown that these assumptions have very little effect on the results.

Another type of divergence results when lateral control response to pilot inputs is reversed. In this case, the lateral control divergence parameter (LCDP) is used. This parameter is derived from an approximation of the ϕ/δ_a transfer function (Reference 7)

$$\frac{\phi}{\delta_a} = \frac{C_{y_{\delta_a}} C_{\ell_\beta} s + C_{\ell_{\delta a}} C_{n_\beta} - C_{\ell_\beta} C_{n_{\delta a}} + \frac{b}{c} C_{y_{\delta_a}} \left(C_{\ell_\beta} C_{n_r} - C_{\ell_r} - C_{n_\beta}\right)}{\left(\frac{b}{c}\right)^2 f(s)} \tag{4}$$

where f(s) is the approximated lateral open-loop characteristic equation. For this derivation only the steady state terms (f(o)) are considered. For normal roll response, $\phi/\delta_a < 0$. Since $C_{y_{\delta a}}$ is generally <<1 it can be neglected and the transfer function becomes

$$\frac{\phi}{\delta_a} = \frac{C_{\ell_{\delta a}} C_{n_\beta} - C_{\ell_\beta} C_{n_{\delta a}}}{\left(\frac{b}{c}\right)^2 f(o)} \tag{5}$$

Multiplying by $\left(\frac{b}{c}\right)^2 f(o)$ (a positive value) equation 5 reduces to

$$C_{\ell_{\delta a}} C_{n_\beta} - C_{\ell_\beta} C_{n_{\delta_a}} < 0$$

For almost all configurations the control derivative $C_{\ell_{\delta a}}$ is negative, therefore dividing by it will reverse the inequality and yield the final result

$$LCDP = C_{n_\beta} - C_{\ell_\beta} \frac{C_{n_{\delta a}}}{C_{\ell_{\delta a}}} \tag{6}$$

where positive values indicate normal response to roll control and negative values indicate a reversed response. If an aileron-rudder interconnect (ARI) system is used then equation 6 becomes

$$LCDP = C_{n_\beta} - C_{\ell_\beta} \frac{C_{n_{\delta a}} + K\, C_{n_{\delta r}}}{C_{\ell_{\delta a}} + K\, C_{\ell_{\delta r}}} \tag{7}$$

where K is the ARI gain.

The equations used for calculating $\dot{q}$, $\dot{r}$, and $\dot{p}$ come from the moment equations of the equations of motion. By neglecting all of the rate terms and assuming that the moments are generated entirely by control deflection, the following relationships can be obtained:

$$\dot{q} = \frac{\bar{q}\, S\, \bar{c}}{I_y}\, C_{m_{\delta e}} \cdot \delta e \tag{8}$$

$$\dot{r} = \frac{\bar{q}\, S\, b}{I_z}\, C_{n_{\delta r}} \cdot \delta r \tag{9}$$

$$\dot{p} = \frac{\bar{q}\, S\, b}{I_x}\, C_{\ell_{\delta a}} \cdot \delta a \tag{10}$$

Because of inertia coupling the maximum roll rate (about the stability axis) allowable is determined by the amount of available pitch control. When rolling about the velocity vector, especially at high angles-of-attack, a typically fuselage-heavy fighter aircraft will experience a nose-up pitching moment

(Reference 8). For an aircraft symmetrical about the X-Z plane, and if again the assumption is made that the only source of pitching moment is from control deflection, the steady state pitching moment equation becomes

$$(I_z - I_x)\, pr + \bar{q}\, S\, \bar{c}\, C_{m_{\delta e}} \cdot \delta e = 0 \tag{11}$$

Substituting

$$p = p_s \cos \alpha \tag{12}$$

and

$$r = p_s \sin \alpha \tag{13}$$

into equation 11 gives

$$(I_z - I_x)\, p_s^2 \cos \alpha \sin \alpha + \bar{q}\, S\, \bar{c}\, C_{m_{\delta e}} \cdot \delta e = 0 \tag{14}$$

Using nose-down control deflections it is possible to determine the maximum stability axis roll rate allowable without incurring an uncontrollable pitch-up. This relationship is given by

$$p_s = \left[\frac{-2\, \bar{q}\, S\, \bar{c} \cdot C_{m_{\delta e}} \cdot \delta e}{(I_z - I_x) \sin 2\alpha} \right]^{1/2} \tag{15}$$

CHAPTER 5

RESULTS AND DISCUSSION

Static Stability and Control

Vertical Tail Geometry.- Figure 10 shows the effect of the centerline and twin tails on longitudinal characteristics. The centerline tail has no effect on lift or pitching moment but the twin tails reduce $C_{L_{MAX}}$ and also increase the magnitude of the pitching moment. Earlier work with a similar configuration (Reference 1) indicated that this decrease in lift and the related increase in pitching moment were due to early vortex bursting caused by the twin tails.

A comparison of the effect of the centerline tail and the twin tails on lateral-directional characteristics is made in figure 11. The centerline tail maintains directional stability (C_{n_β}) until $\alpha = 25°$ and continues to provide a stabilizing increment until $\alpha = 30°$. With further increases in angle of attack the centerline tail is destabilizing. Past $\alpha = 50°$ the stabilizing effects of the forebody (Reference 1) dominate. The twin tails have a stabilizing effect throughout the angle-of-attack range tested. There is a sharp loss of directional stability, however, between $\alpha = 15°$ and 20°. Adverse sidewash from the wing leading edge vortex system is the most probable cause of this reduced stability region.

Dihedral effect ($-C_{\ell_\beta}$) is also affected by the tail geometry. At low angles of attack both tail configurations produced an increase in effective dihedral. Between $\alpha = 30°$ and 50° the centerline tail is destabilizing because of the adverse side force on the tail which is well above the aircraft center of gravity. When this destabilizing rolling moment is added to the low stability caused by asymmetric vortex bursting on the wing a region of instability results

from α = 35° to 40°. The twin vertical tails force the wing vortices to burst symmetrically, which greatly increases the effective dihedral between α = 25° and 40°.

A comparison of the longitudinal characteristics for the aft and forward swept twin tails is made in figure 12. The forward swept tails had a slight effect on lift between α = 16° and 19° causing a more abrupt break in the pitching moment curve. The longitudinal position of the forward swept tail had very little effect on either lift or pitching moment.

Figure 13 shows the effect of forward and aft swept vertical tails on lateral-directional characteristics. The forward swept tails show improvement in directional stability over the aft swept tails in the region from α = 15° to 20°. Above α = 20°, however, the aft swept tails provide much more directional stability. With the forward swept tails in the aft position (this position gives the forward swept tails approximately the same tail volume as the aft swept tails) directional stability is increased to match the aft swept tails at the lower angles of attack. Laterally, all three configurations maintain adequate levels of stability with minimal differences between them except between α = 10° and 20° where the aft swept tails exhibits less effective dihedral.

The effect of spanwise location of the twin vertical tails on longitudinal and lateral-directional characteristics was also investigated and the results are shown in figures 14 and 15, respectively. For both positions the trailing edge extension was removed and the aft swept tails used. The lift curve showed no change except for a slight increase in maximum lift for the outboard tail position. This position also caused the pitch-up to occur 2° earlier than the inboard position (α = 12°). Spanwise location of the vertical tails had no effect on dihedral. There was an improvement, however, in directional stability

by moving the tails outboard. Directional stability is maintained with the outboard tails through the region from $\alpha = 15°$ to 25° where the inboard tails exhibit a reduction in stability.

Of all the vertical tail parameters varied, tail cant angle had the most impact on both the longitudinal and lateral-directional characteristics. The longitudinal characteristics are presented in figure 16. Cant angle has little effect on lift with the exception of the 30° outboard cant. This configuration exhibited an increase in maximum lift. This can be attributed to the additional lifting surface created with such an extreme outboard cant. Vertical tail cant angle also had a noticeable effect on the pitching moment. For all cases the initial pitch-up occurred at about $\alpha = 8°$. Both the inboard and outboard 30° cants affected pitching moment more than either 15° cant. The 30° outboard cant increased the severity of the pitch-up and caused a stable pitching moment slope past $\alpha = 15°$. The 30° inboard cant, however, decreased the pitch-up but delayed a stable pitching moment slope until $\alpha = 20°$ as did the other configurations. In Reference 1, which showed this same trend, it was found that the cant angle, not the spanwise location of the vertical tail tip, affected the pitching moment characteristics. Extensive flow visualization studies will be needed to fully understand the fluid mechanics involved.

Figure 17 shows the effect of vertical tail cant angle on the lateral-directional stability of this configuration. Below 14° angle of attack, cant angle has little effect on directional stability. Past $\alpha = 14°$, canting the tails outboard, much like moving the vertical tails spanwise more outboard, increased directional stability. Effective dihedral was also increased, showing the same trends as shown by the tests of Reference 1. Canting the tails inboard had the opposite effect. That is both lateral and directional stability were

decreased. Since in sideslip the windward wing vortex moves more inboard it is not surprising that inboard canting of the tails places the vertical tails in an unfavorable flow field.

Leading Edge Flaps.- The deflection of a three-segmented leading edge flap was investigated primarily to reduce the pitch-up tendencies. Figure 18 shows the pitching moment data for the various flap settings tested. For all configurations, the static margin increased at low angles of attack, and the pitch-up was delayed and the severity of the pitch-up reduced. The data indicate that the inboard-most section of flap contributes most to this improvement in pitching moment characteristics apparently by reducing the strength of the wing vortex. The data of figure 19 indicate that by scheduling the leading edge flaps (that is, using a different flap deflection at each angle of attack) it is possible to reduce the severity of the pitch-up significantly without sacrificing directional stability. Decreasing the severity of the pitch-up by scheduling flap deflection would reduce the amount of nose-down control needed between $\alpha = 8°$ to 15° and allow the clean configuration to be flown in the angle-of-attack range used for supersonic cruise flight ($\alpha \leq \sim 6°$).

Longitudinal Control.- Four methods for obtaining adequate pitch control were tested: flaps on the trailing edge extensions, use of the ailerons as flaps, horizontal tails, and canards. The data on these configurations are presented in figures 20 through 26.

The trailing edge extension could utilize either a plain flap or a slotted flap, both capable of deflecting up and down. Figure 20 (a) shows the control power available for the slotted flap while figure 20 (b) shows the same data for the plain flap. The two concepts provide the same amount of nose-up pitching moment, allowing the configuration to be trimmed to about 40° angle of attack.

The plain flap, however, provides slightly more nose-down moment than the slotted flap at the lower angles of attack and maintains this advantage until $C_{L_{MAX}}$.

The use of ailerons deflected symmetrically was investigated as a primary source of pitch control and also as an augmentation of the trailing edge extension flaps. The data of figure 21 show that the ailerons produce a little more than half the pitching moment that the plain trailing edge extension flap produced. This coupled with rapid loss in effectiveness past $\alpha = 15°$ makes the ailerons unacceptable for primary pitch control. However, in conjunction with the flaps, the ailerons increase the available pitch power in the lower angle-of- attack range where additional pitch control was needed. The ailerons also extended the trim angle of attack to 42°, approximately 7° beyond the stall.

By removing the trailing edge extensions, it is possible to add horizontal tails to the configuration. A clear benefit of the horizontal tail configuration is that it reduces the severity of the pitch-up around $\alpha = 15°$ (figure 22). The available control power using the horizontal tail is comparable to that of the flap-aileron combination and the maximum trim angle of attack is increased to 44°. Unfortunately, on this configuration the use of horizontal tails requires either fuselage mounted twin vertical tails or a single centerline vertical tail, both of which have poor lateral-directional stability characteristics (Reference 1).

The use of canards required the addition of a fairing along the upper surface of the inlet area. The effects of this fairing on the longitudinal and lateral-directional characteristics were examined before the canards were added. The longitudinal data (figure 23) show a slight increase in lift around $C_{L_{MAX}}$, but a much greater change in pitching moment. The addition of the fairing

decreases longitudinal stability below $\alpha \approx 12°$, delays the stable break in the pitching moment curve to a higher angle of attack ($\alpha = 38°$) and increases the nose-up pitching moment considerably. All of these results are undesirable, making adequate nose-down control a problem and high angle-of-attack stability poor. The fairing had far less effect on lateral-directional stability (figure 24). Directional stability is unchanged and effective dihedral is actually increased in some regions.

Figure 25 shows that when the canards are deflected to -40° to produce a nose-down moment, C_{n_β} becomes negative at a lower angle of attack than for a 0° deflection. While there is some effect on C_{ℓ_β}, the changes are not significant. The data of figure 26 indicate that even with a deflection of -40° the canard is unable to produce a nose-down moment past $\alpha = 12°$.

Directional control.- Adequate rudder power, especially at high angles of attack, is always a concern with high performance aircraft. Four concepts for directional control were evaluated as part of this investigation: an all moving centerline tail, a conventional rudder, a rudder with a forward swept hinge line, and tip rudders. The work of Reference 9 has shown these last two concepts to be very effective at high angles of attack.

The all moving centerline tail, as was expected, was extremely powerful at low angles of attack (figure 27) with more than adequate yaw control from 10° of deflection. More yawing moment can be generated with a 30° deflection, but the effectiveness drops off sharply past $\alpha = 25°$ as the tail becomes shielded by the wing and fuselage. For angles of attack above 30° the larger deflection provides only as much yawing moment as the 10° deflection. All rudder power with either deflection is lost by $\alpha = 45°$.

A comparison of the conventional rudder on the aft swept tail and the forward swept rudder on the forward swept tail is presented in figure 28. The

forward position of forward swept tail (FST) coincided with the position of the aft swept tail (AST) while the rearward position of the FST was designed to have approximately the same tail volume as the AST. The difference in the magnitude of rudder power between the AST and the FST is a result of the larger rudder area of the FST. The conventional rudder starts to lose effectiveness at α = 15° because the flow becomes increasingly parallel to the rudder hingeline until by α = 40° all rudder power is lost. The forward swept rudders, however, are designed to keep the flow more perpendicular to the rudder hingeline at high angles of attack and are therefore able to maintain adequate directional control well past $C_{L_{MAX}}$.

Tip rudders (figure 5) were also studied for obtaining high angle-of-attack directional control. As angle of attack increases the hingeline of the tip rudders becomes more perpendicular to the freestream. As a result of this, the tip rudders start to become effective at α = 15° (figure 29) as the rudder on the AST starts to lose its effectiveness. The tips rudders maintain good yaw control until the stall where, like the FST rudders, effectiveness is reduced. With a larger rudder on the AST, it should be possible to achieve good levels of yaw control by using the AST rudders and the tip rudders in conjunction with each other.

Lateral Control.- Two basic concepts were evaluated for roll control: ailerons and deflectable wing tips. Both constant chord ailerons and ailerons with unswept hingelines were tested and the results are presented in figure 30. There is very little difference between the two concepts. Both start losing effectiveness past α = 15° because of spanwise flow on the wing, and by α = 30° neither are very effective. Up until this point, however, the constant chord ailerons supply slightly more rolling moment.

In order to take advantage of the spanwise flow on the wing, deflectable wing tips with a hingeline that is about 45° to the wing chord were tested. Below α= 20° these deflectable wing tips provided slightly less rolling moment than the constant chord ailerons (figure 31). After a small drop in effectiveness just past α = 20°, however, the deflectable wing tips maintain an almost constant amount of roll control to an angle of attack of 60° while the ailerons continue to lose effectiveness. By combining these two concepts it is possible to provide sufficient rolling moment throughout the angle-of-attack range.

Estimated Flight Dynamics

The last three sections of this chapter deal with the flight dynamics and maneuverability predicted using the static data. The configuration used to obtain these results was the forward swept tails using both ailerons and trailing edge extension flaps for pitch control and both ailerons and deflectable wing tips for roll control (table 1). Data on the current aircraft used for comparison of maneuverability were obtained from Reference 10.

Departure Resistance.- The data of figure 32 show that this configuration should be very resistant to yaw departure (nose slice). Positive values of $C_{n_{\beta,dyn}}$ are maintained throughout the angle-of-attack range tested. In general, $C_{n_{\beta,dyn}}$ becomes more positive with increasing angle of attack except between α = 16° and 24° and in the post-stall region (α > 35°). Even though C_{n_β} is negative or very small for this configuration between α = 20° and 46°, the stable values of C_{ℓ_β} from α = 0° to 60° should be enough to prevent a nose slice from occurring.

Control Reversal.- When adverse yawing moment due to aileron deflection becomes too high, too much sideslip is generated and control response to a pilot roll input will be reversed. This control reversal is predicted when LCDP (as defined in Chapter 4) becomes negative. For ailerons only, this configuration will experience a reversed response to roll inputs past $\alpha = 20°$. In order to prevent this, it is necessary to use rudder deflection to offset the adverse yaw due to aileron deflection. This can be accomplished manually by the pilot or by using an aileron-rudder interconnect (ARI) system. The ARI system provides a proportional amount of yaw control for a given roll input in order to ensure proper control response. With the proper ARI gain ($K = 0.35$), correct response to pilot roll commands can be maintained until $\alpha = 45°$ (figure 33).

Maneuverability. The maneuverability of an aircraft is generally measured by how fast it can turn about its three axes. This requires a complete data base, such as that used in simulation studies, and knowledge of restrictions that could limit the maximum allowable rates and accelerations. A less exact method is to use the equations presented in Chapter 4 to calculate the maximum rate accelerations that can be commanded using a constant velocity and altitude. This gives an indication of how fast an aircraft can initiate a turn. Figure 34 presents the rate accelerations that can be commanded for a current highly maneuverable aircraft (Aircraft A) and the configuration of this study (Aircraft B).

The pitch rate acceleration data of figure 34(a) show that below the stall (both aircraft stall at $\alpha = 35°$) Aircraft A can initiate a pitch attitude change faster than Aircraft B. Aircraft B, however, is capable of higher pitch rate acceleration beyond the stall. Also, Aircraft B shows little change in pitch rate acceleration with changing angle of attack. This will provide the pilot

with virtually the same longitudinal response to his pitch control inputs throughout this angle-of-attack range.

The results of the yaw rate acceleration calculations are presented in figure 34(b). The data indicate that Aircraft A is capable of generating higher yaw rate accelerations than Aircraft B throughout the angle-of-attack range tested. A consequence of lower attainable yaw rate acceleration for Aircraft B will be lower effectiveness of a stability augmentation system (SAS) in the yaw axis. Exactly how important this is depends upon the basic airframe static and dynamic stability characteristics.

Figure 34(c) shows the roll rate acceleration capabilities of the two aircraft. Aircraft A is capable of initiating a roll rate quicker than Aircraft B below the stall whereas the opposite is true above the stall. It is common in the region approaching the stall and above for aircraft with highly swept wings to exhibit wing rock tendencies. The higher roll rate acceleration capability of Aircraft B in this angle-of-attack range will allow more effective use of artificial stabilization to prevent this wing rock.

High performance aircraft, which are typically fuselage heavy, tend to pitch-up when rolling about the aircraft velocity vector (stability axes) because of inertia coupling. This places a limitation on the maximum stability axes roll rate that can be maintained. This maximum roll rate, as shown in equation 15, is related to the amount of nose-down longitudinal control power available to overcome the pitch-up caused by inertia coupling. A detailed description of inertia coupling can be found in Reference 8. Figure 35 shows the results of this evaluation for the test configuration and current aircraft. Below the stall, Aircraft A is limited less by inertia coupling than Aircraft B, allowing Aircraft A to make quicker rolls about the velocity vector. In the

post-stall region, however, Aircraft B is able to sustain a higher roll rate that is almost constant throughout the remainder of the angle-of-attack range.

CHAPTER 6

SUMMARY OF RESULTS

The results of this investigation to evaluate conventional and unusual control concepts and to study the effect of tail geometry on stability and control may be summarized as follows:

1. A twin vertical tail configuration offered the best overall stability characteristics based on static data.

2. It was found that spanwise location and cant angle of the vertical tails could be used to tailor longitudinal and lateral-directional stability.

3. It was possible to use scheduling of leading edge flaps to reduce the severity of the pitch-up without sacrificing supersonic cruise performance.

4. A combination of trailing edge extension flaps and symmetric aileron deflection provided good pitch control past the stall angle of attack.

5. Rudders on forward swept tails provided the simplest method of obtaining high angle-of-attack yaw control. Results also indicate that it could be possible to achieve the same amount of yaw control with an aft swept tail rudder plus a tip rudder.

6. Deflectable wing tips, which take advantage of wing spanwise flow, were found to provide good roll control when used in conjunction with ailerons.

7. Static stability levels indicated that the forward swept tail configuration should be highly departure resistant.

8. It was shown that proper aileron-rudder interconnect gains could postpone roll control reversal from $\alpha = 20°$ to $\alpha = 45°$ and prevent a control induced departure.

10. Based on attainable rate accelerations and taking into account limitations resulting from inertia coupling, the maneuverability of the forward swept tail configuration was close to that of a highly maneuverable aircraft below the stall and exceeded that of the current aircraft in the post-stall region.

REFERENCES

1. Klein, J. R.; Walck, K. J.; and Hahne, D. E.: "Airframe Component Effects on the Aerodynamic Stability and Control Characteristics of a Supersonic Cruise Fighter Aircraft at High Angles of Attack". AIAA-84-2110, August 1984.

2. Grafton, Sue B.; and Nguyen, Luat T.: "Wind Tunnel Free-Flight Investigation of a Model of a Cranked-Arrow-Wing Fighter Configuration". NASA TP-2410, March 1985.

3. Wood, R. M.; Miller, D. S.; Hahne, D. E.; Neidling, L.; and Klein, J.: "Status Review of a Supersonically Biased Fighter Wing-Design Study". AIAA-83-1857, July 1983.

4. Johnson, J. L.; Grafton, S. B.; and Yip, L. P.: "Exploratory Investigation of the Effects of Vortex Bursting on High-Angle-of-Attack Lateral-Directional Stability Characteristics of Highly-Swept Wings". AIAA-80-0463, March 1980.

5. Moul, Martin T.; and Paulson, John W.: "Dynamic Lateral Behavior of High-Performance Aircraft". NACA RM-L58E16, August 1958.

6. Greer, H. Douglas: "Summary of Directional Divergence Characteristics of Several High Performance Aircraft Configurations". NASA TN D-6993, November 1972.

7. Etkin, Bernard: "Dynamics of Atmospheric Flight"; John Wiley & Sons, Inc.; New York, New York, 1972.

8. Nguyen, Luat T.; Gilbert, William P.; and Ogburn, Marilyn E.: "Control-System Techniques for Improved Departure/Spin Resistance for Fighter Aircraft". NASA TP-1689, August 1980.

9. Ransom, Stephen: "Configuration Development of a Research Aircraft with Post Stall Maneuverability", Journal of Aircraft, Vol. 20, No. 7, July 1983.

10. Nguyen, L. T.; Ogburn, M. E.; Gilbert, W. P.; Kibler, K. S.; Brown, P. W.; and Deal, P. L.: "Simulator Study of Stall/Post-Stall Characteristics of a Fighter Airplane With Relaxed Longitudinal Static Stability", NASA TP-1538, December 1979.

Table I Mass and geometric characteristics of the airplane

Weight(Estimated):	
TOGW, lbs	44,000
Moments of Inertia (Estimated):	
I_x, slugs - ft^2	19312
I_y, slugs - ft^2	163899
I_z, slugs - ft^2	176171
Overall Fuselage Length, ft	66.67
Wing:	
Span, ft	36.7
Area, ft	691.9
Mean aerodynamic chord, ft	23.1
Aspect ratio	1.95
Leading edge sweep, deg	65
Swept Aileron:	
Area (one side), ft^2	15.3
Unswept Aileron:	
Area (one side), ft^2	10.1
Deflectable Wingtip:	
Area (one side), ft^2	7.6
Aft Swept Vertical Tail:	
Area (each), ft^2	79.6
Span, ft	9.2
Root chord, ft	14.0
Tip chord, ft	3.2
Aspect ratio	1.06
Leading edge sweep, deg	62.8
Conventional rudder area, ft^2	7.6
Tip rudder area, ft^2	11.7
Forward Swept Vertical Tail:	
Area (each), ft^2	83.7
Span, ft	10.4
Root chord, ft	11.2
Tip chord, ft	4.8
Aspect ratio	1.29
Leading edge sweep, deg	-30
Rudder area, ft^2	18.4

Table I Concluded

Horizontal Tail (all moving):	
Area (each), ft^2	47.67
Span, ft	8.67
Aspect ratio	1.58
Leading edge sweep, deg	42.5
Trailing Edge Extension:	
Length, ft	15.7
Width, ft	4.7
Flap area (each), ft^2	23.0
Canard:	
Area, ft	28.8
Span, ft	5.98
Root chord, ft	7.63
Tip chord, ft	2.08
Aspect ratio	1.24
Leading edge sweep, deg	50

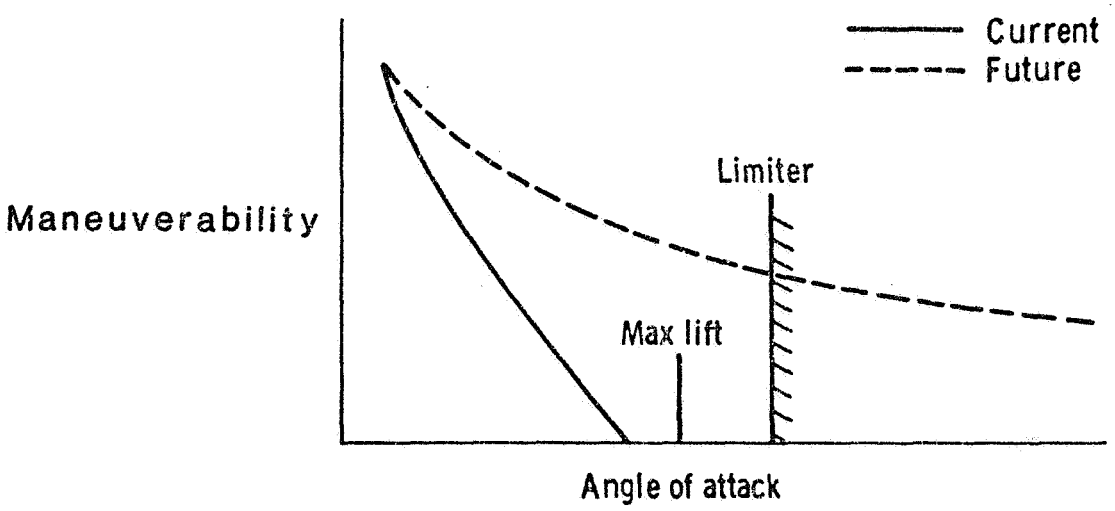

Figure 1. Effect of improved control power on maneuverability.

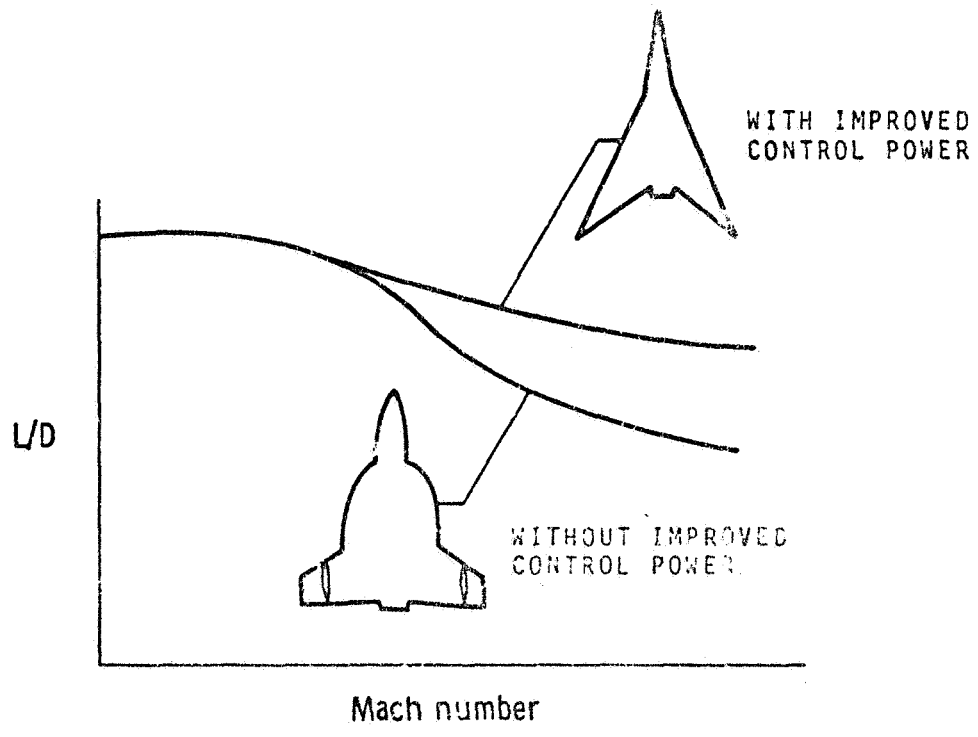

Figure 2. Effect of improved control power on configuration optimization.

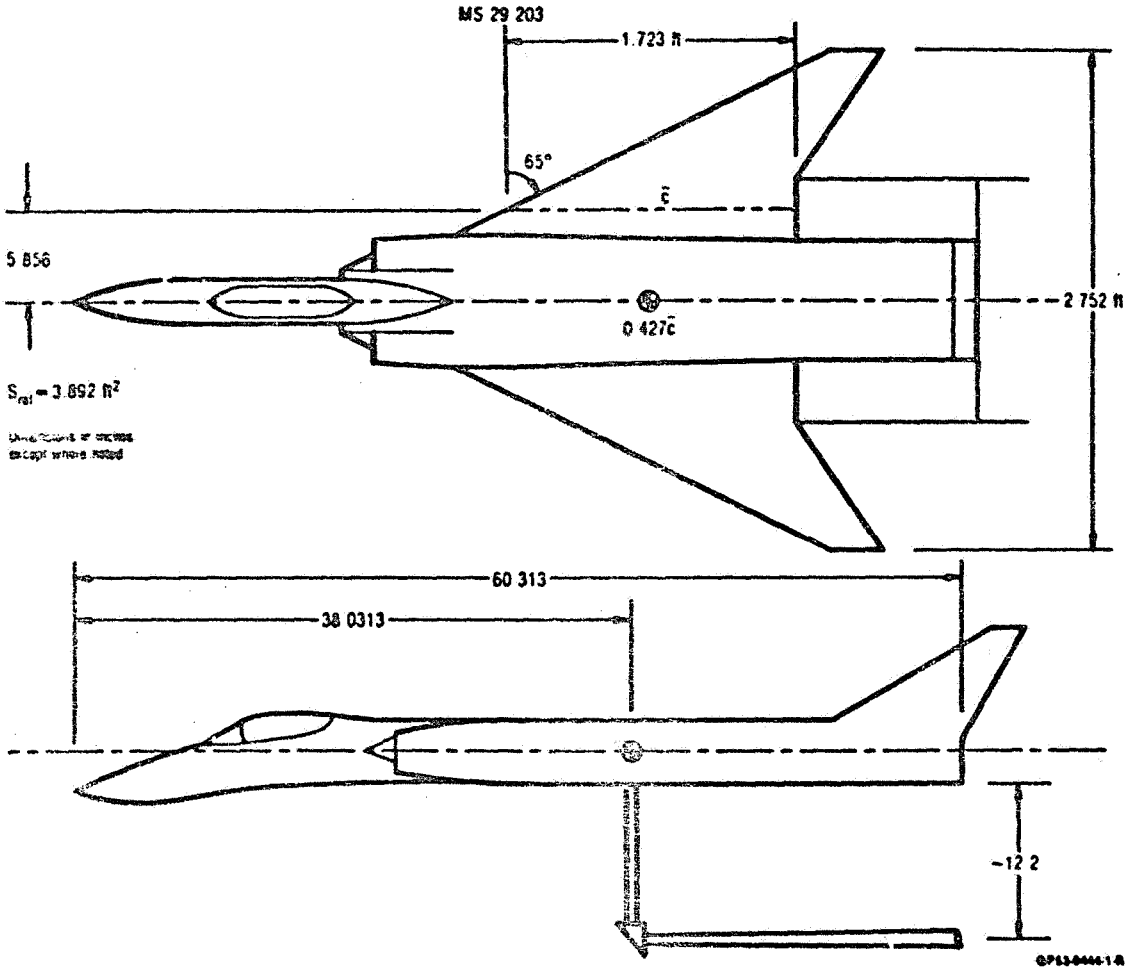

Figure 3. Sketch of basic model configuration.

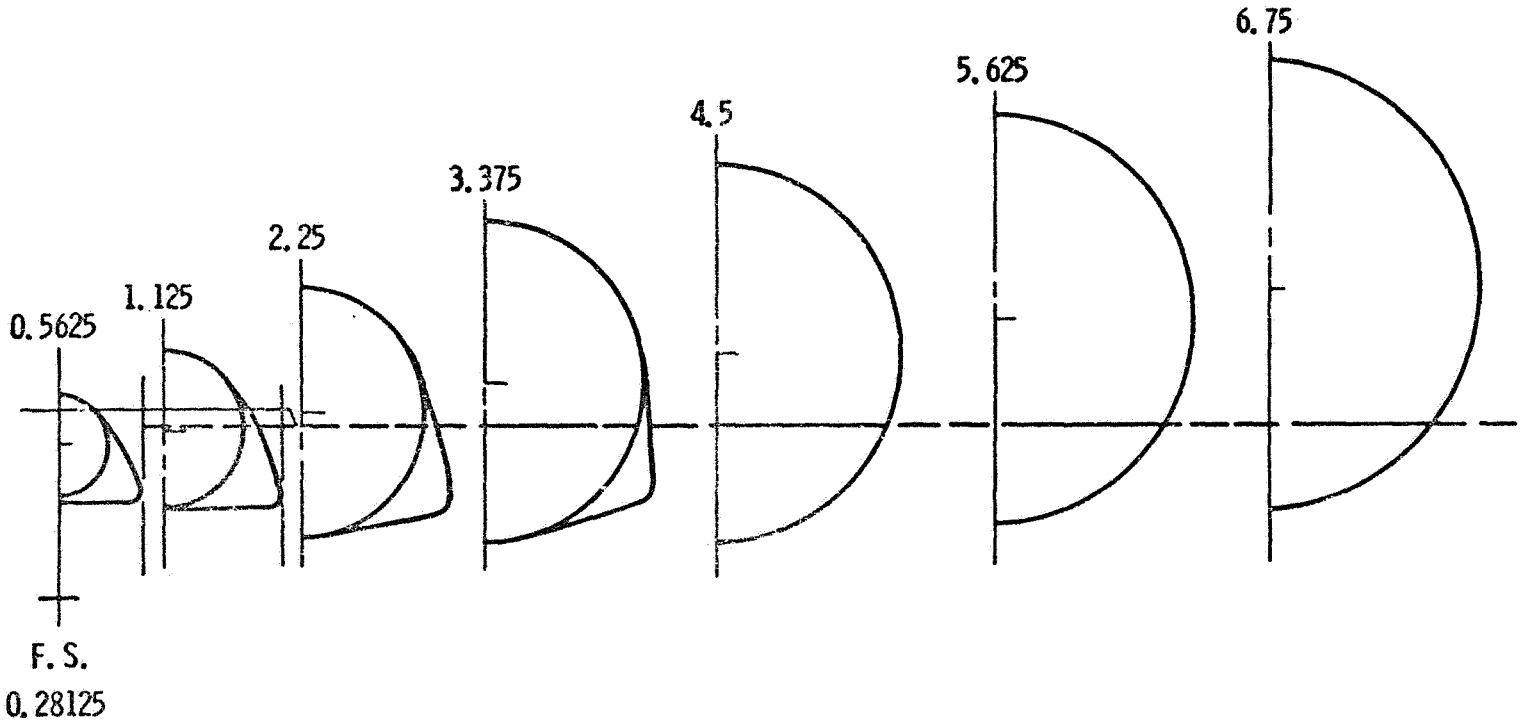

Figure 4. Forebody geometry.

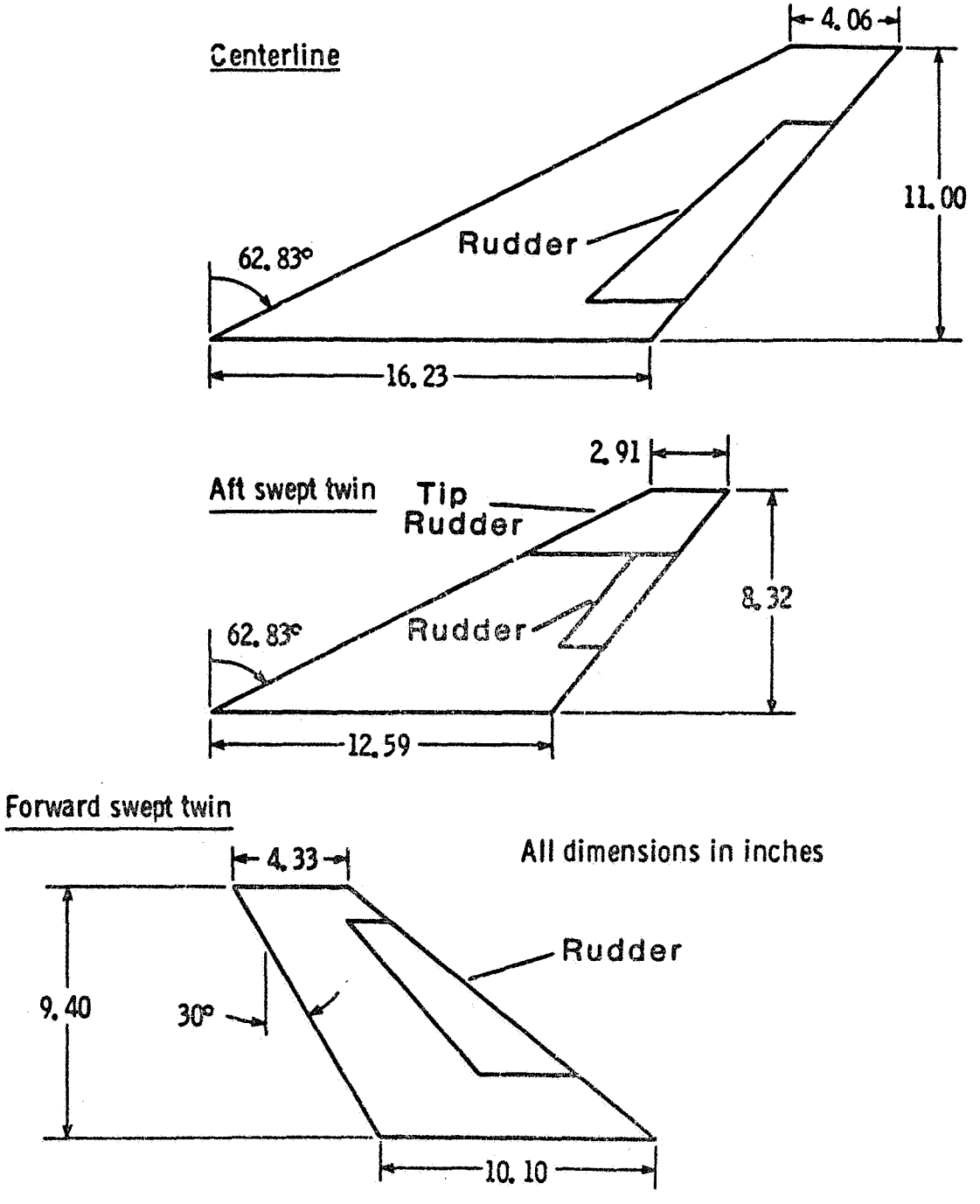

Figure 5. Vertical tail geometry.

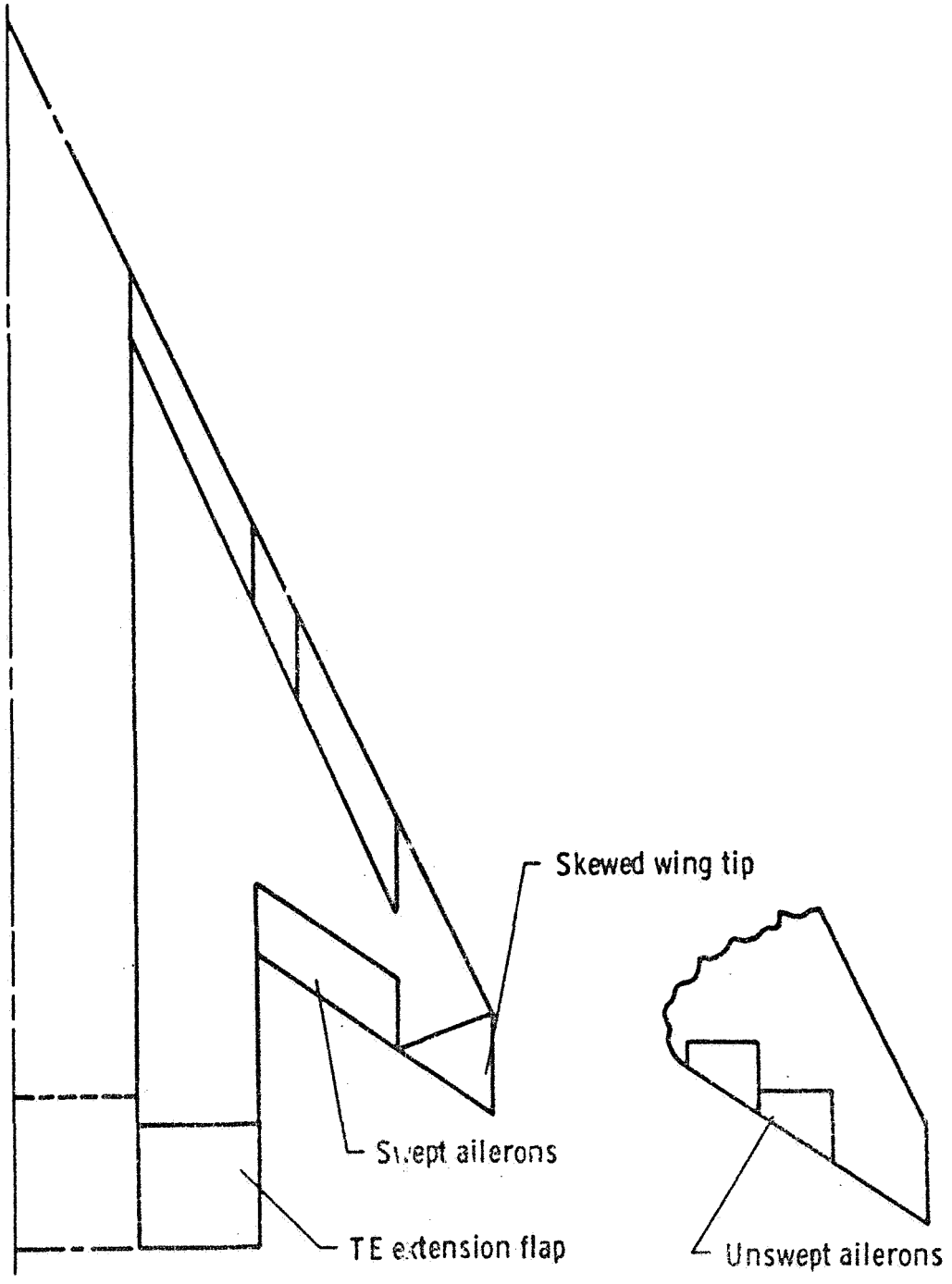

Figure 6. Longitudinal and lateral control surfaces.

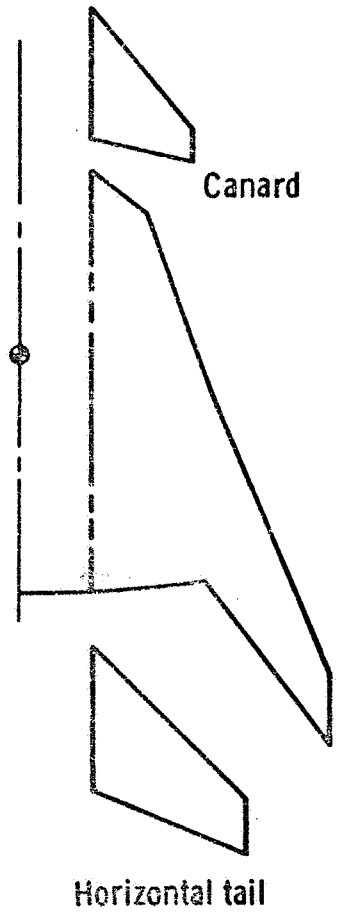

Figure 7. Horizontal tail and canard positions.

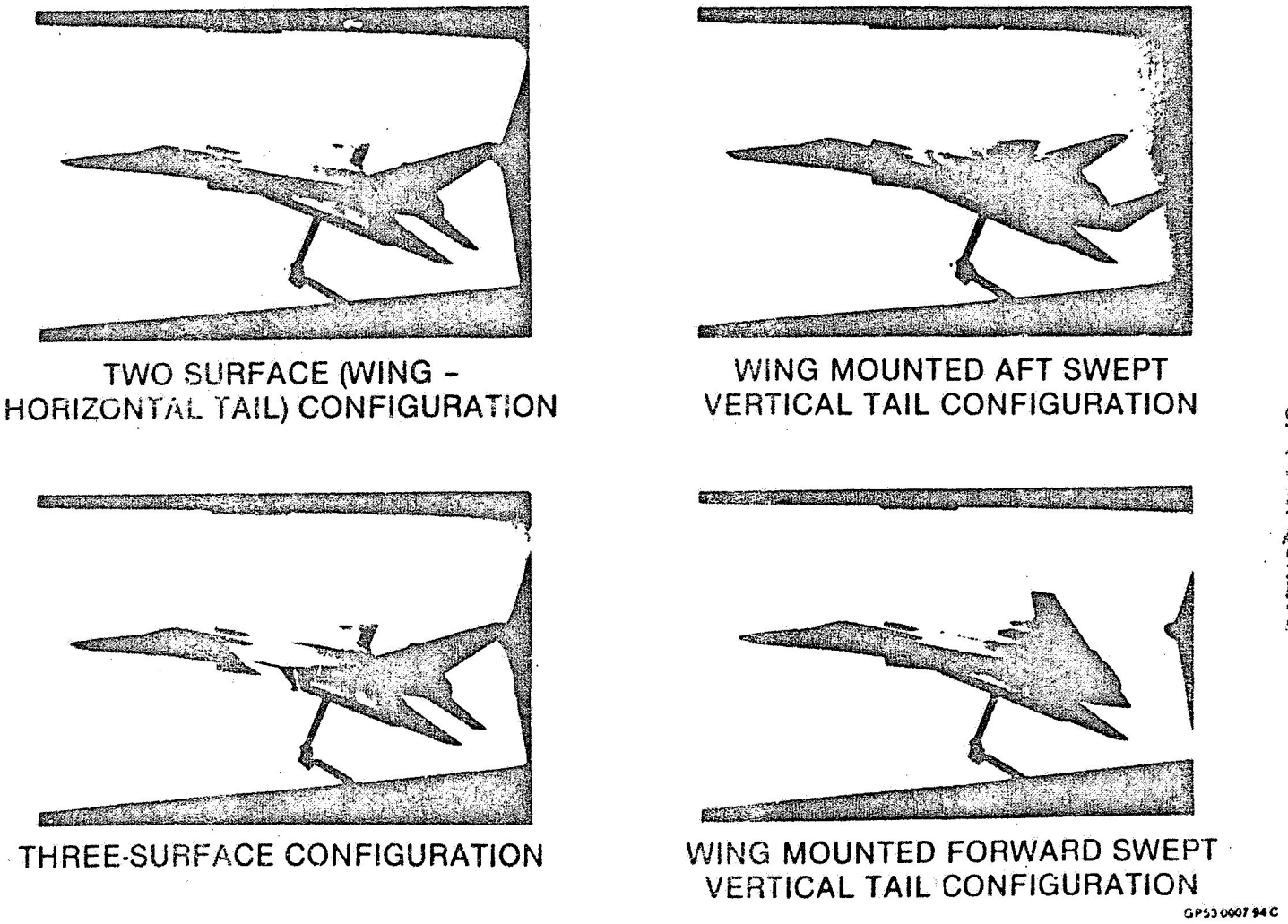

Figure 8. Photograph of model in 12-Foot Low-Speed Tunnel.

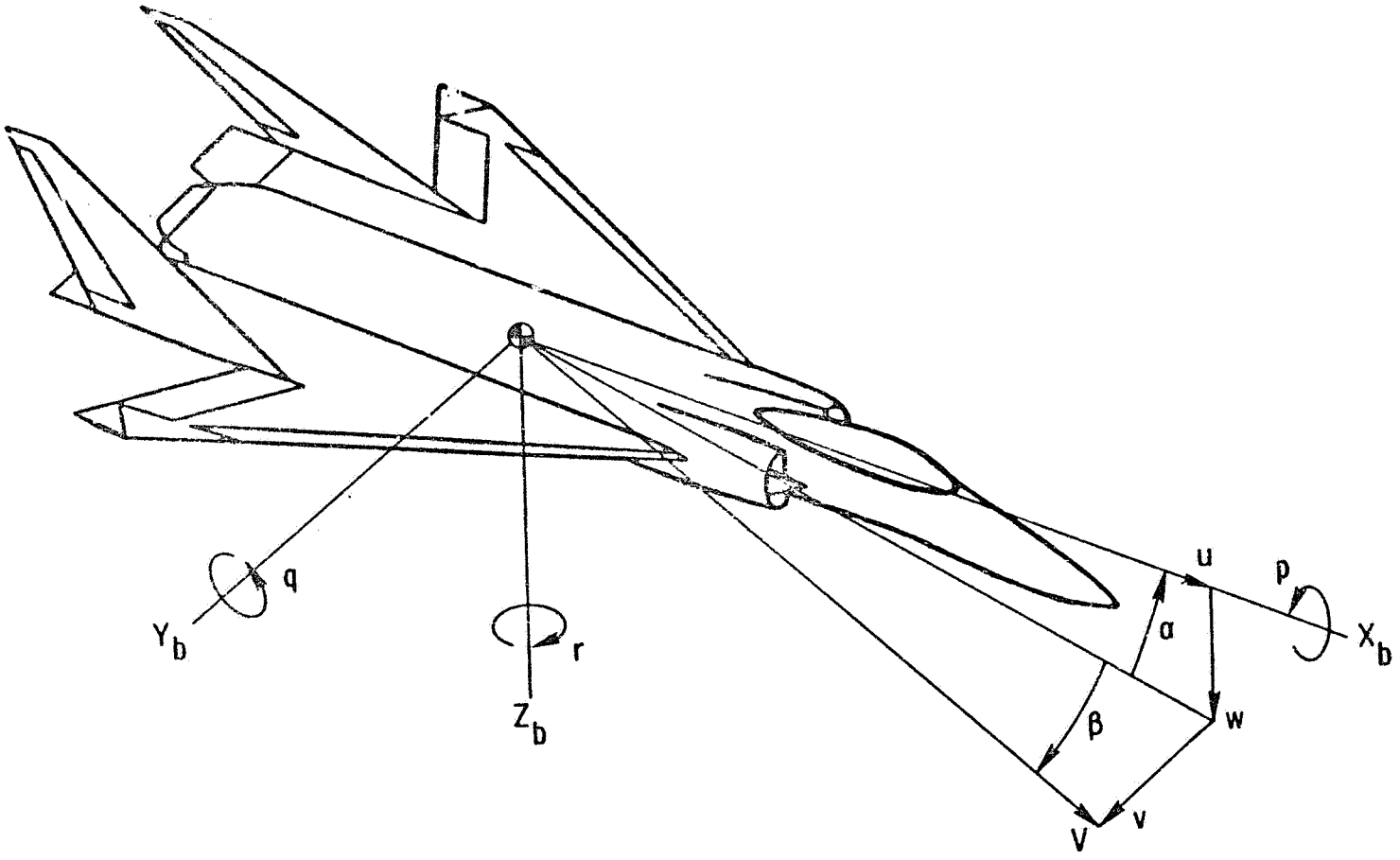

Figure 9. Definition of body axes system.

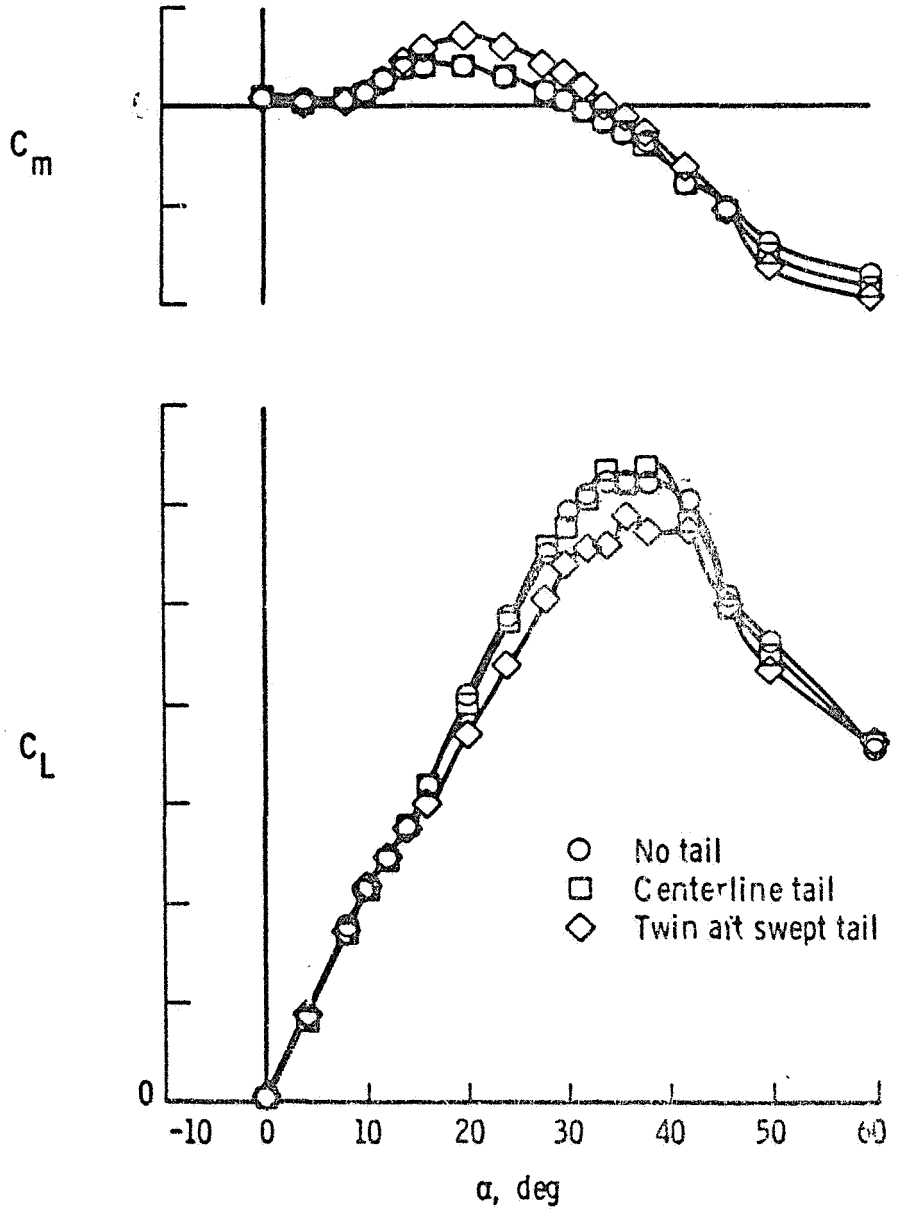

Figure 10. Effect of vertical tail geometry on longitudinal characteristics.

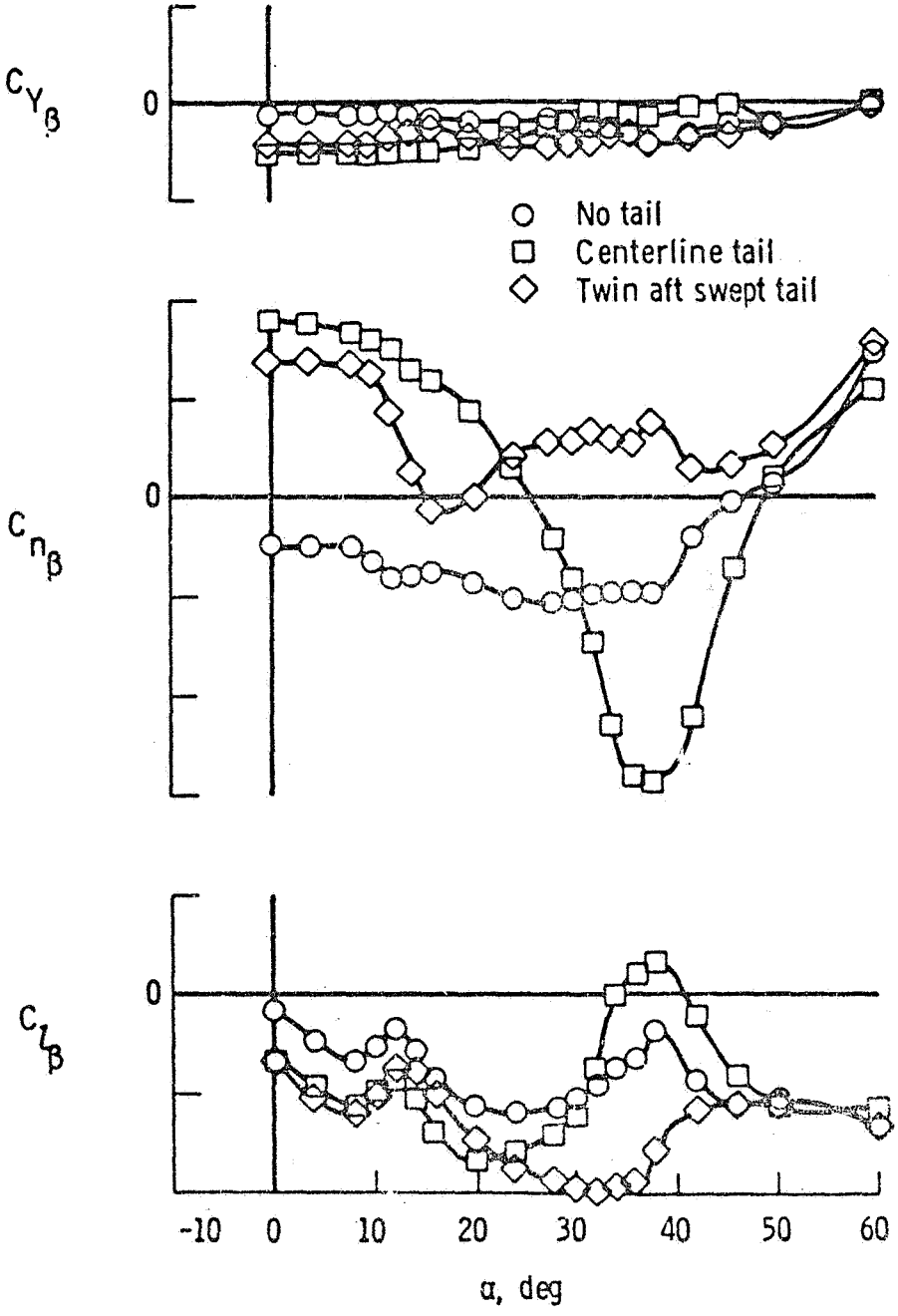

Figure 11. Effect of vertical tail geometry on lateral-directional characteristics.

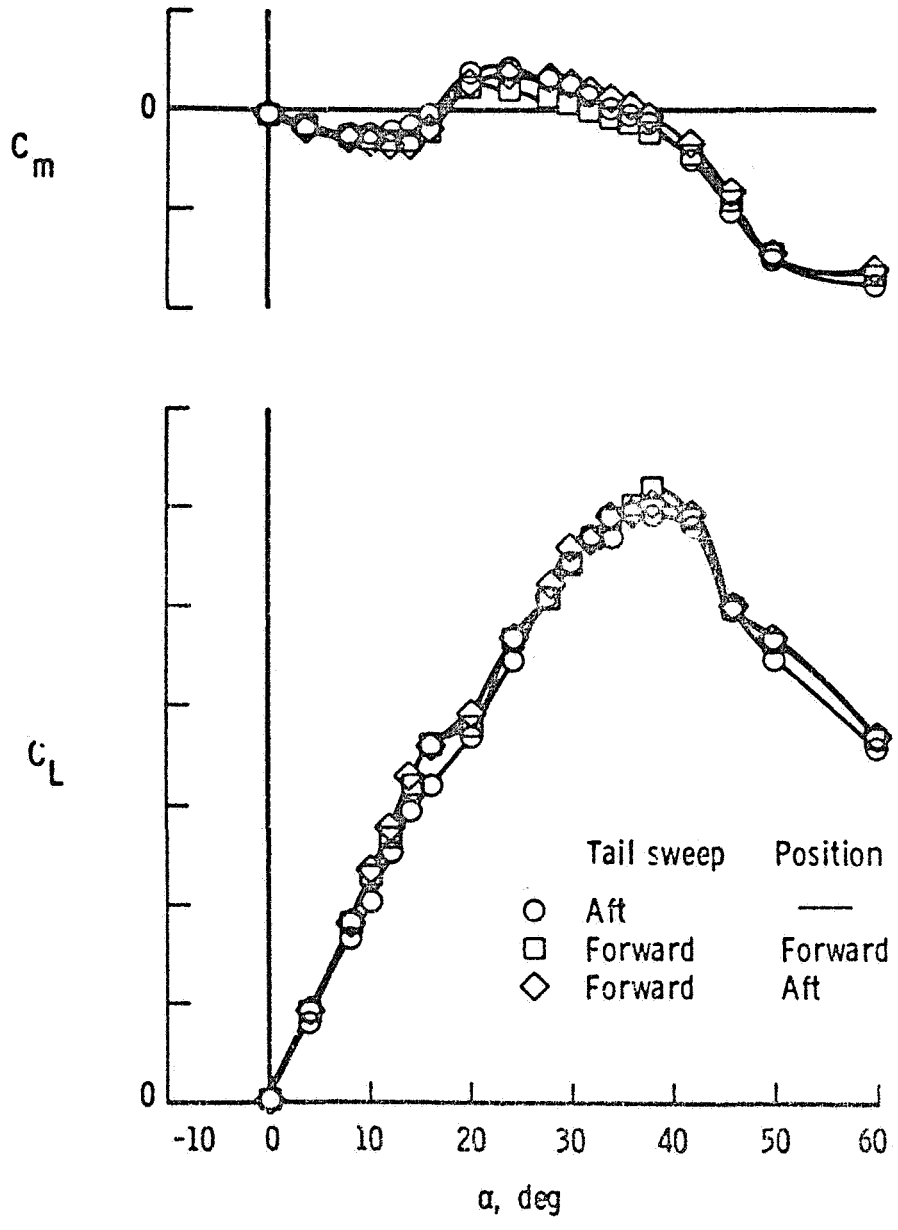

Figure 12. Effect of vertical tail sweep on longitudinal characteristics.

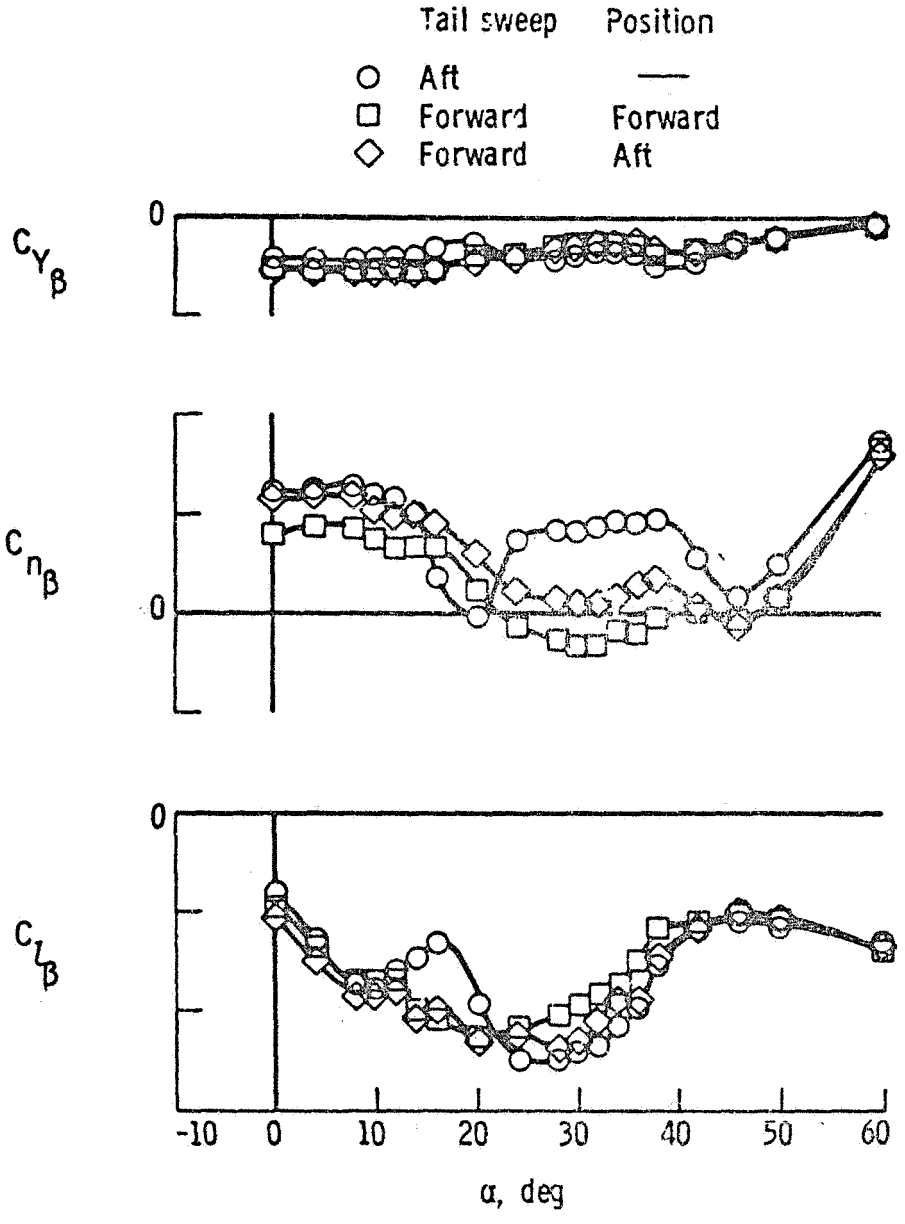

Figure 13. Effect of vertical tail sweep on lateral-directional characteristics.

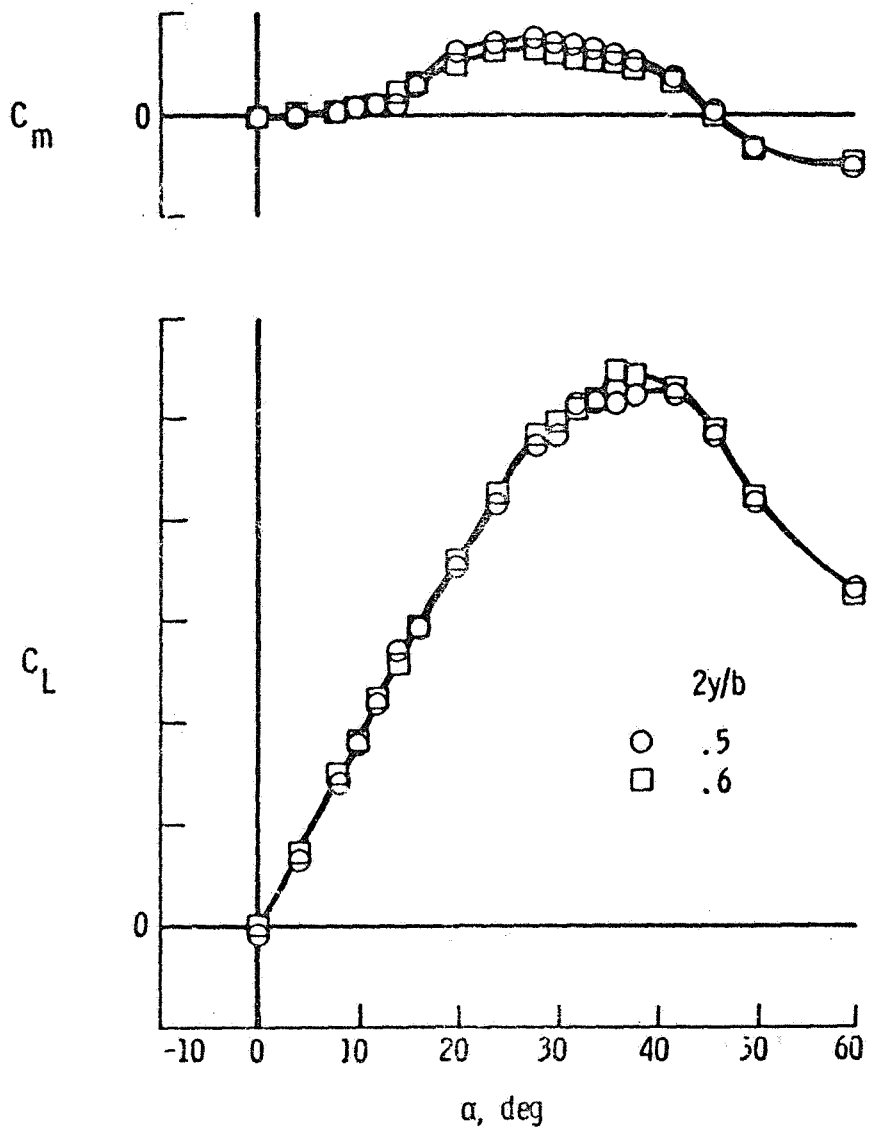

Figure 14. Effect of vertical tail spanwise location on longitudinal characteristics.

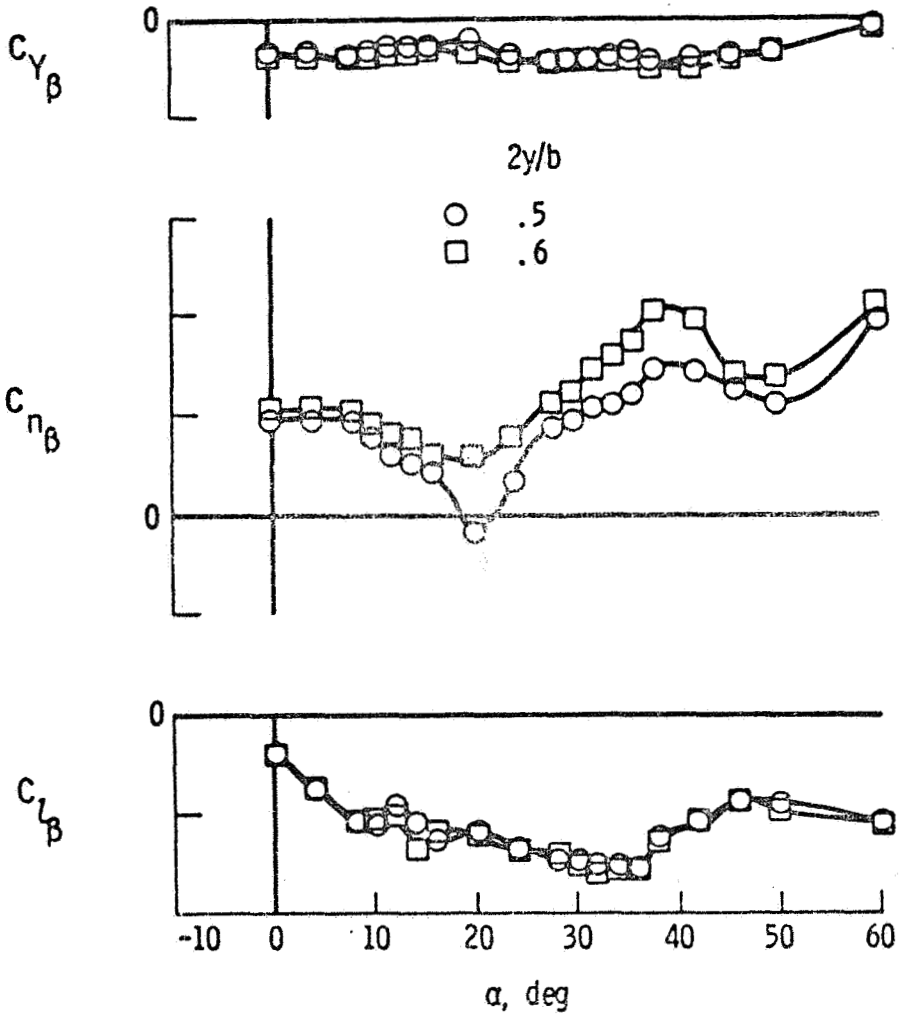

Figure 15. Effect of vertical tail spanwise location on lateral-directional characteristics.

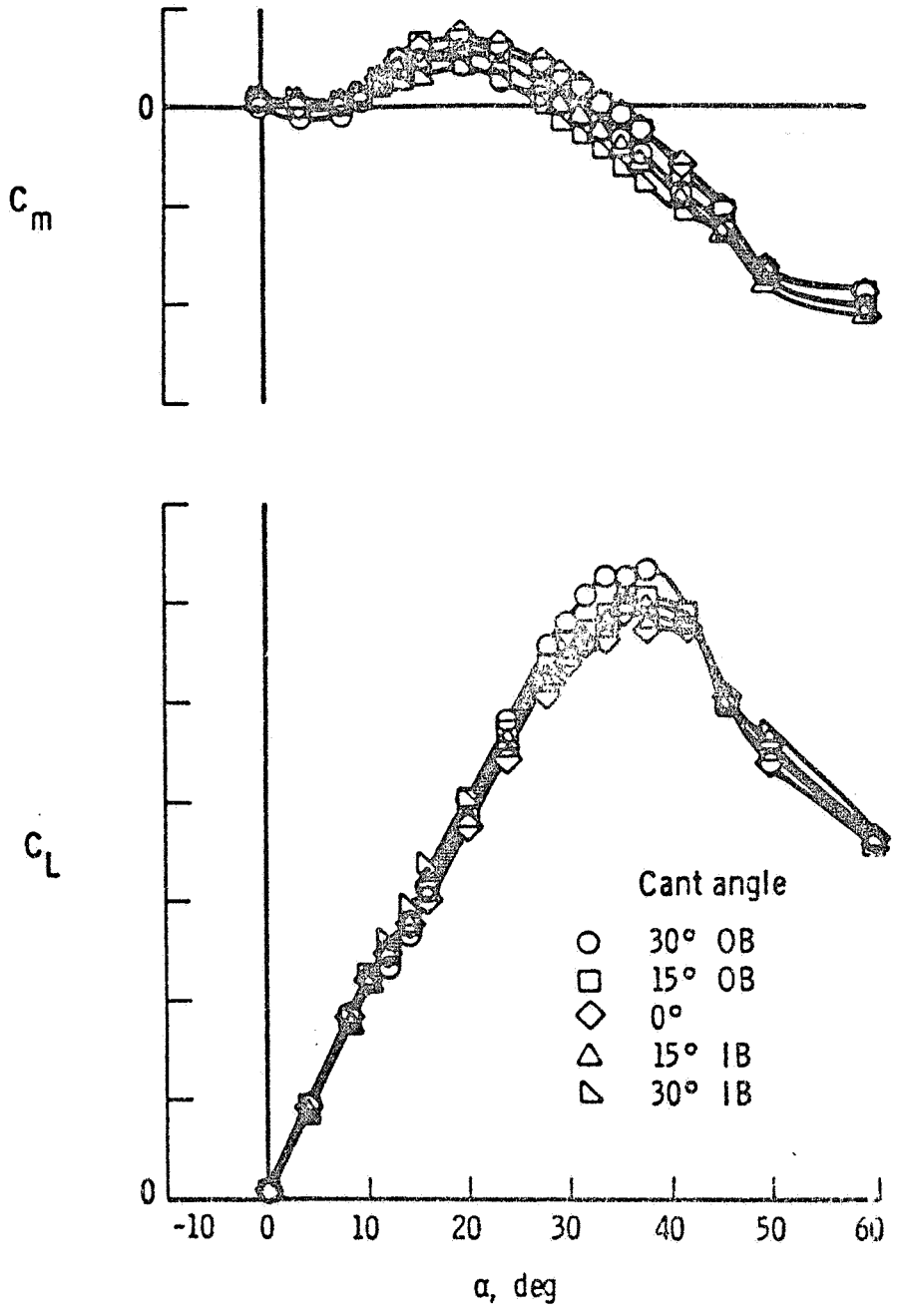

Figure 16. Effect of vertical tail cant angle on longitudinal characteristics.

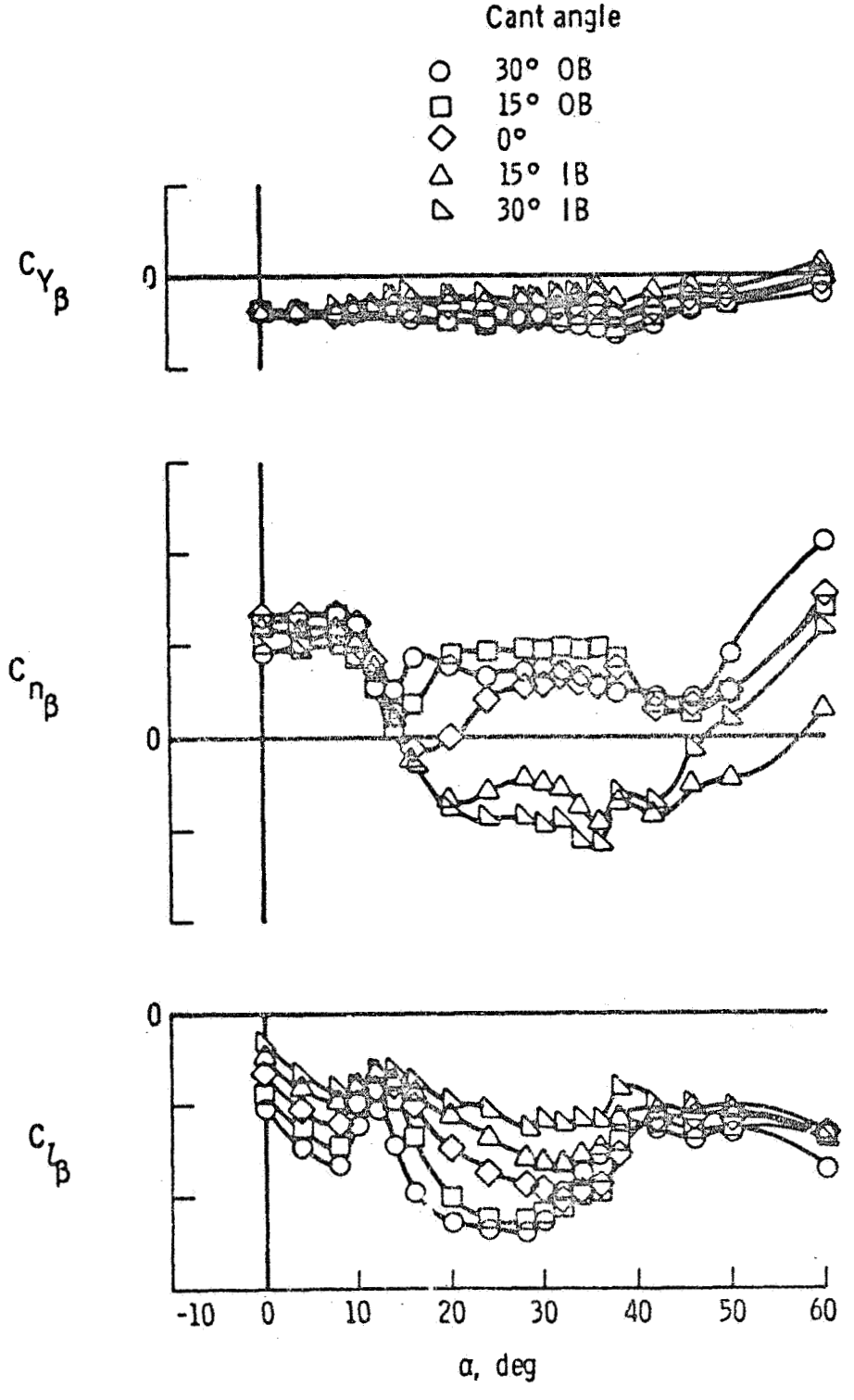

Figure 17. Effect of vertical tail cant angle on lateral-directional characteristics.

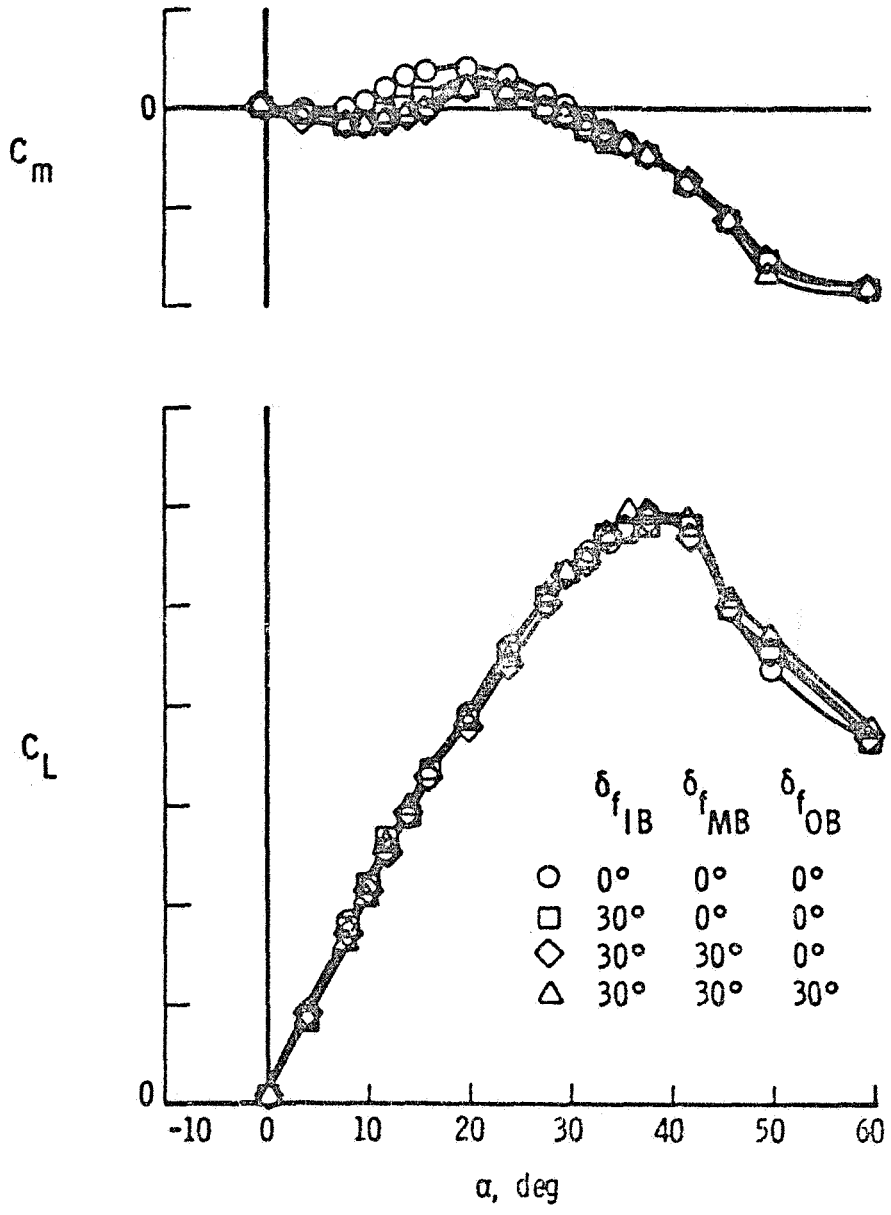

Figure 18. Effect of leading edge flaps on longitudinal characteristics.

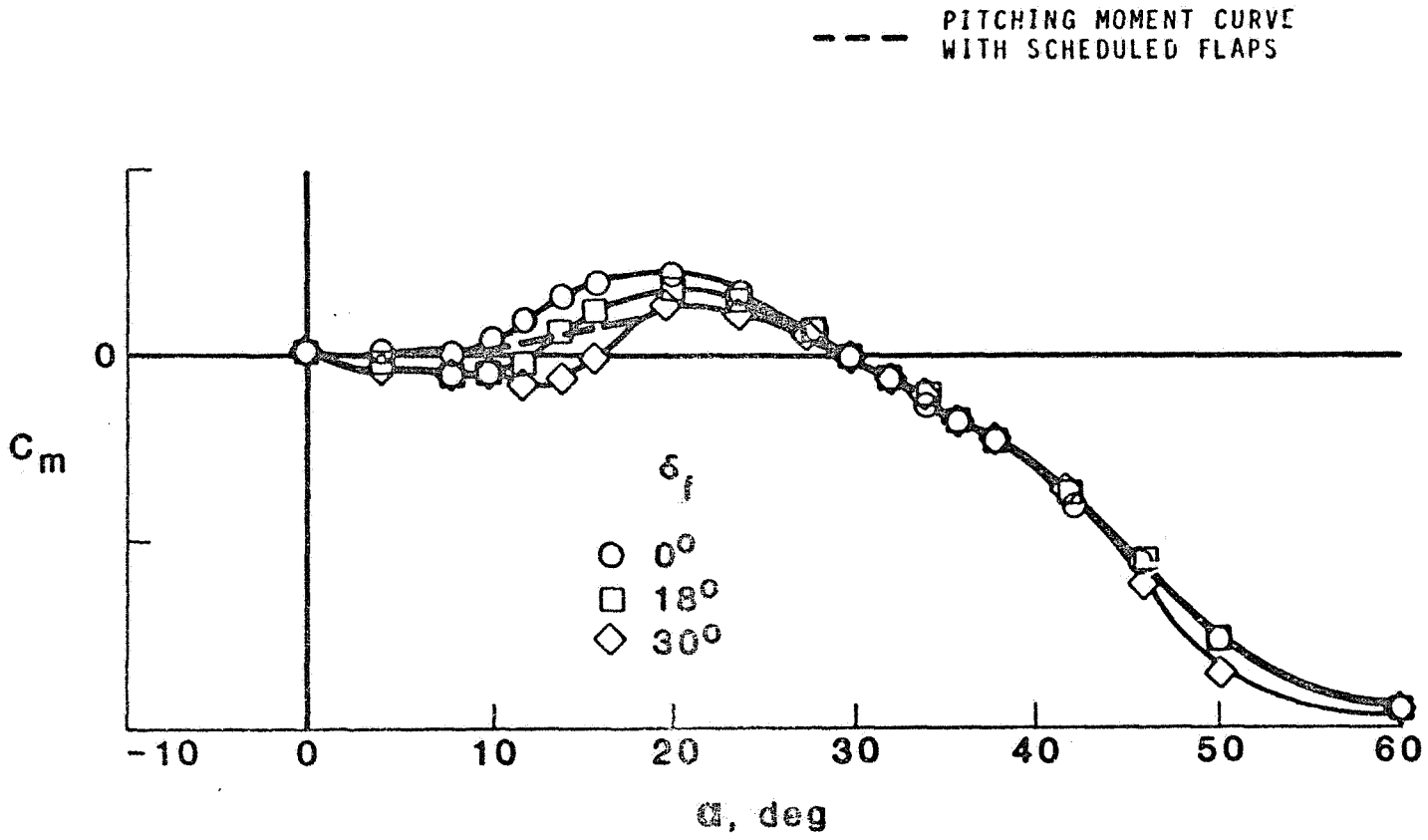

a. Longitudinal characteristics

Figure 19. Effect of scheduled leading edge flaps.

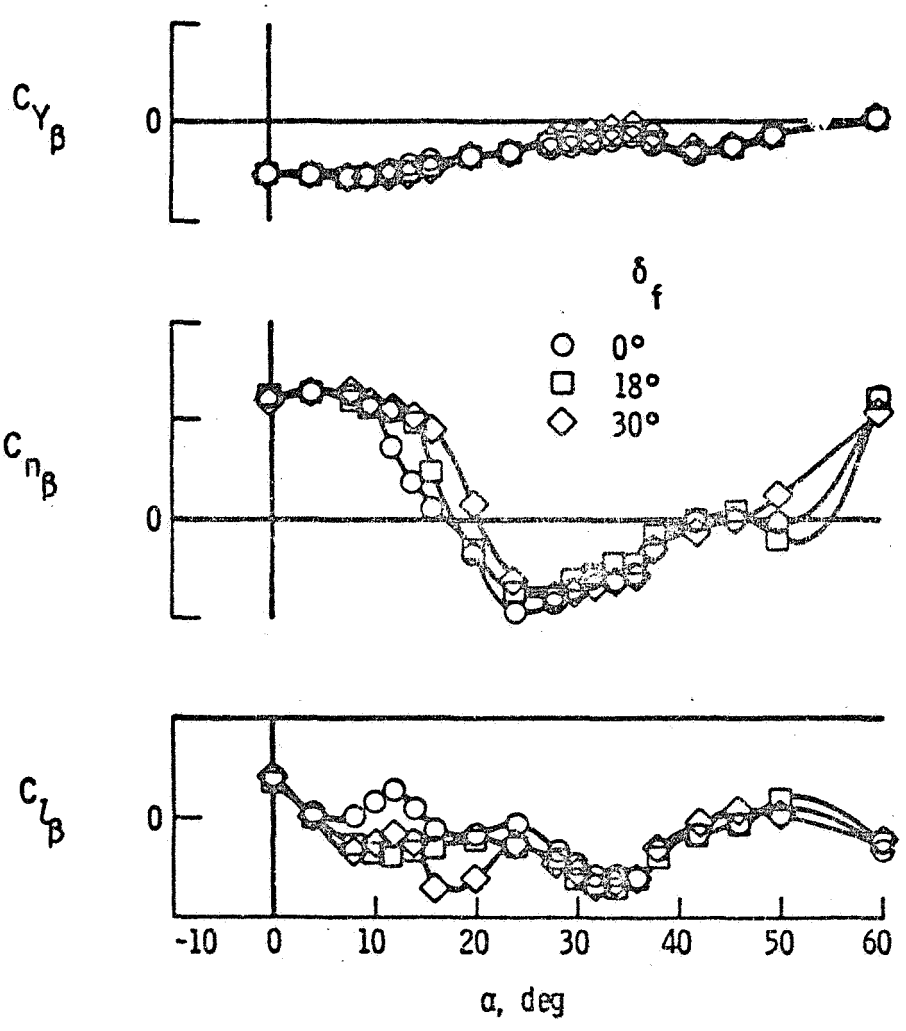

b. Lateral-directional characteristics

Figure 19.- Concluded

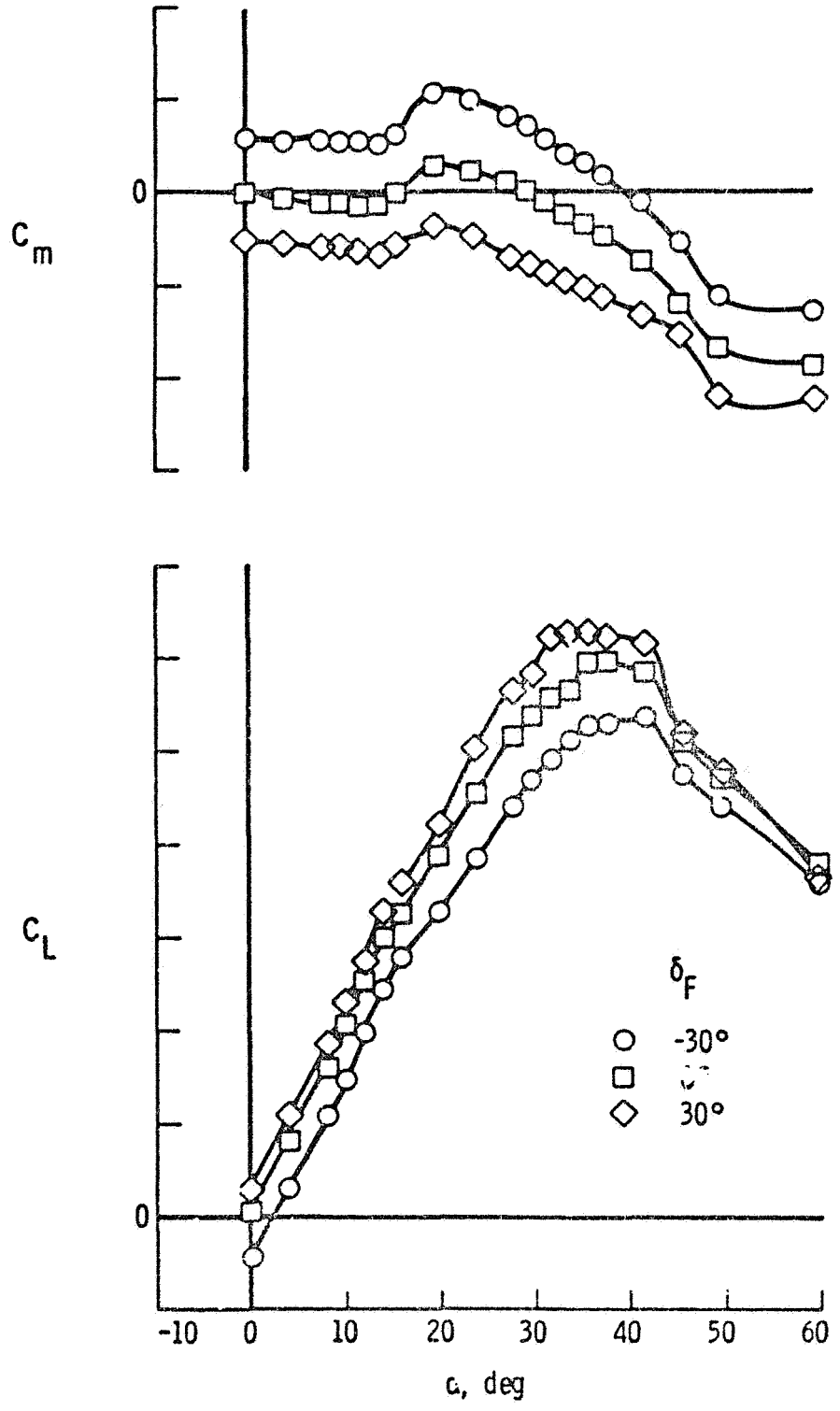

a. Slotted flap

Figure 20. Trailing edge extension flap effectiveness.

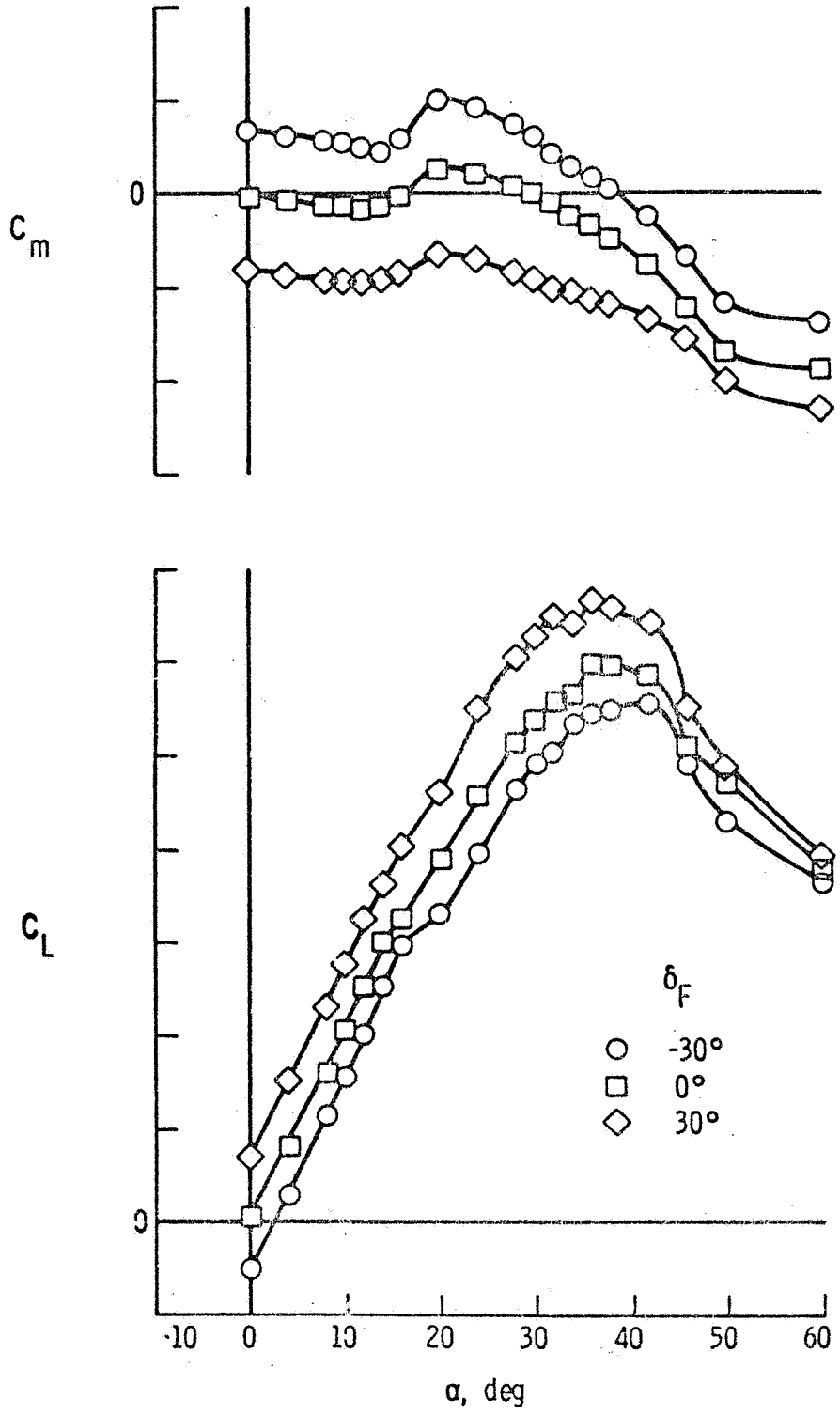

b. Plain flap

Figure 20.- Concluded

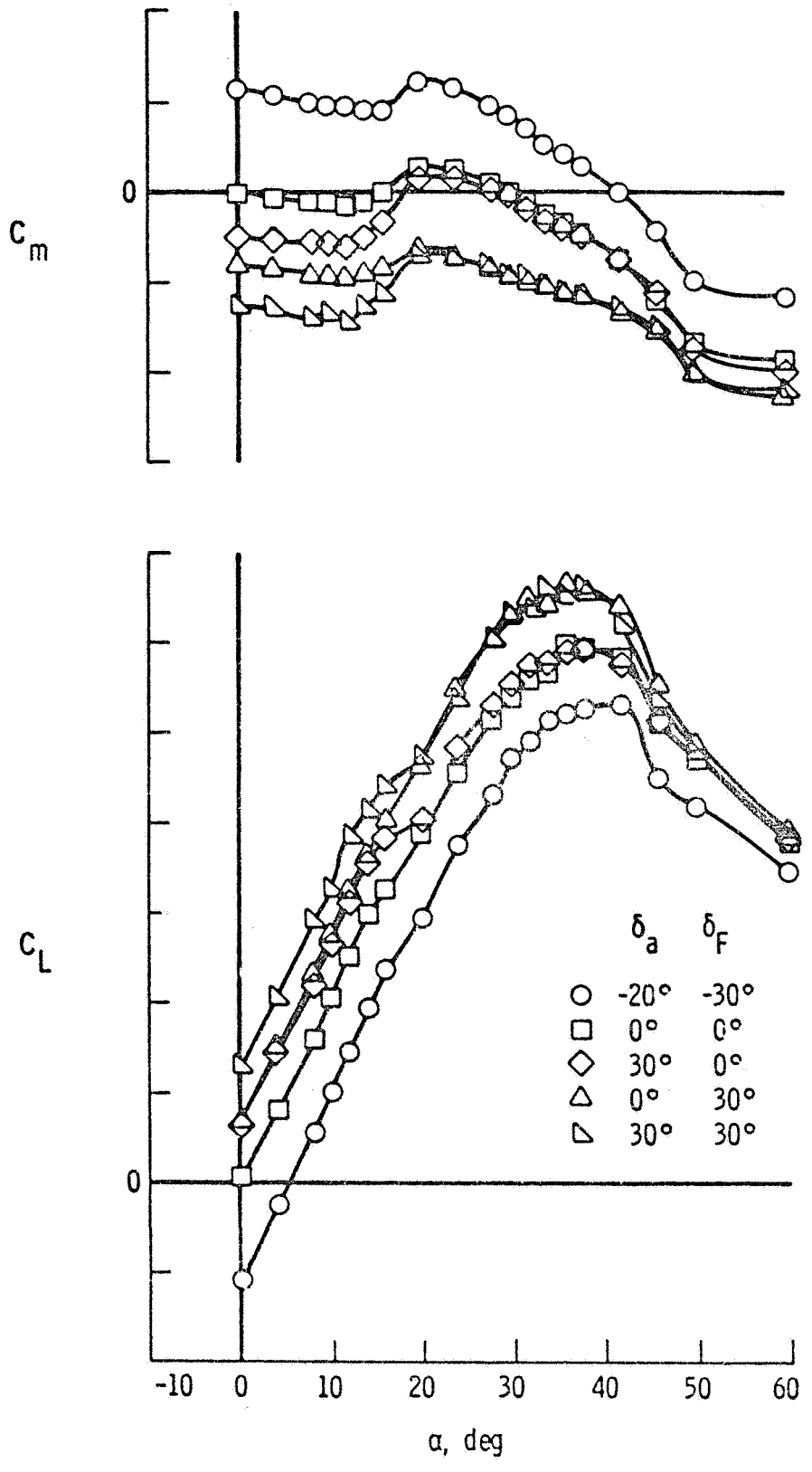

Figure 21. Effectiveness of ailerons for pitch control.

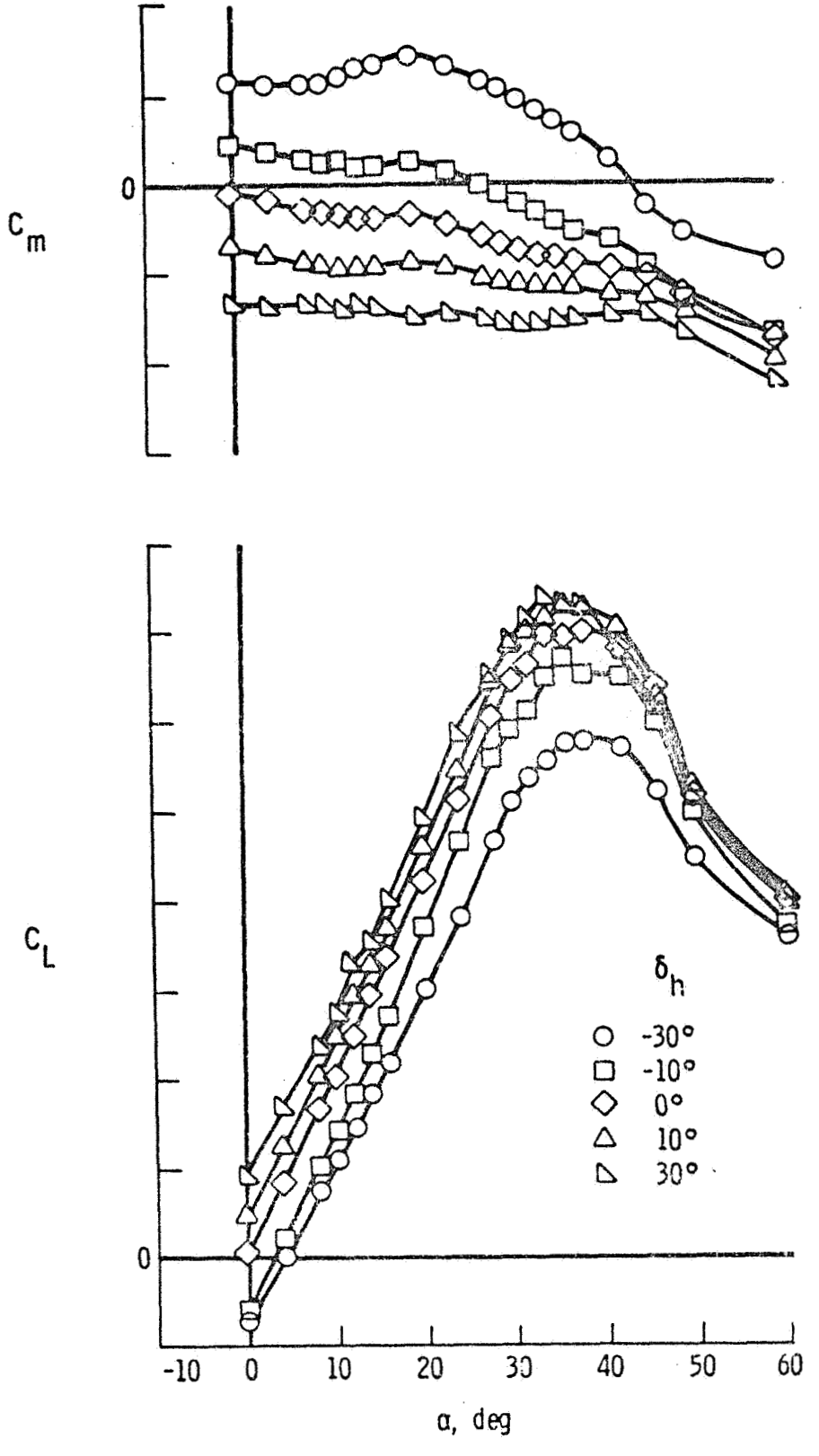

Figure 22. Horizontal tail effectiveness.

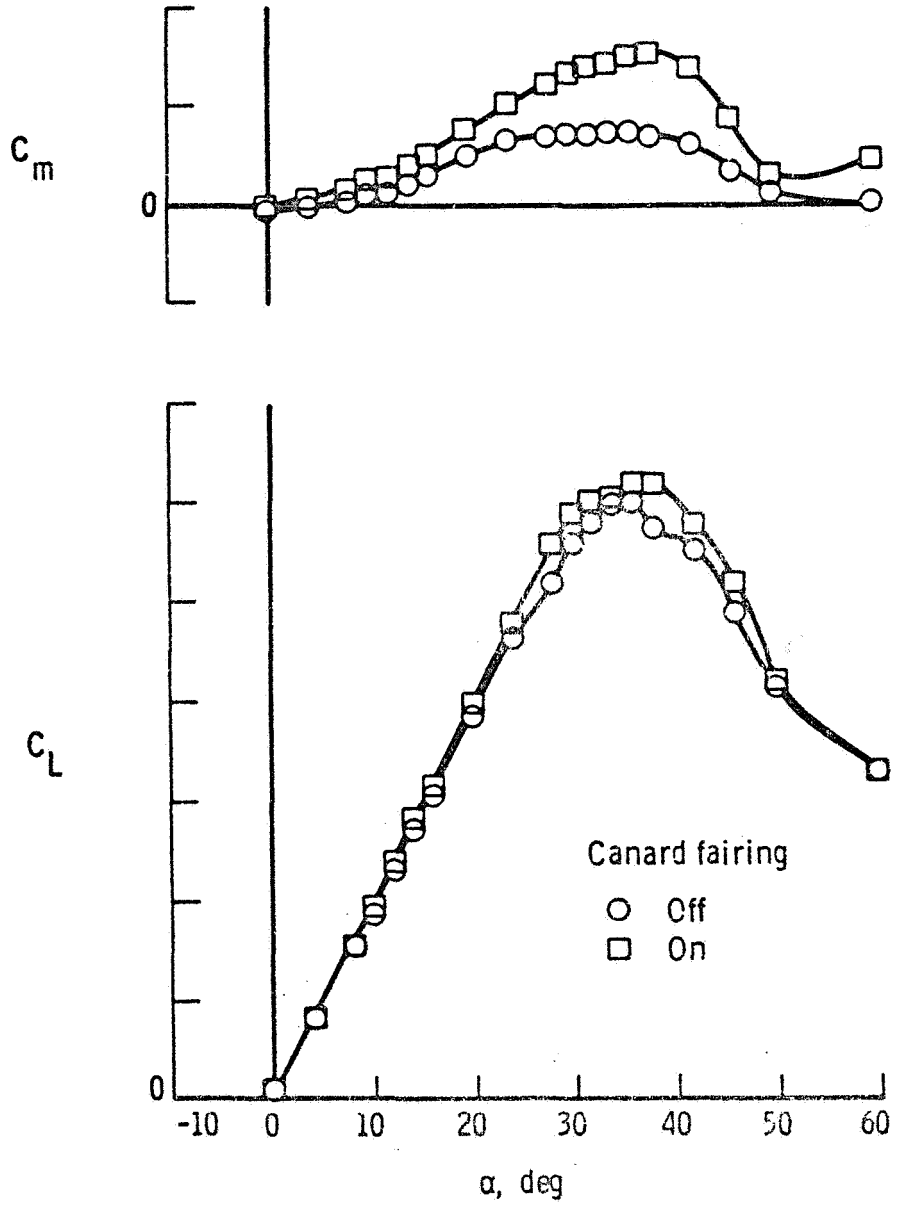

Figure 23. Effect of canard fairing on longitudinal characteristics.

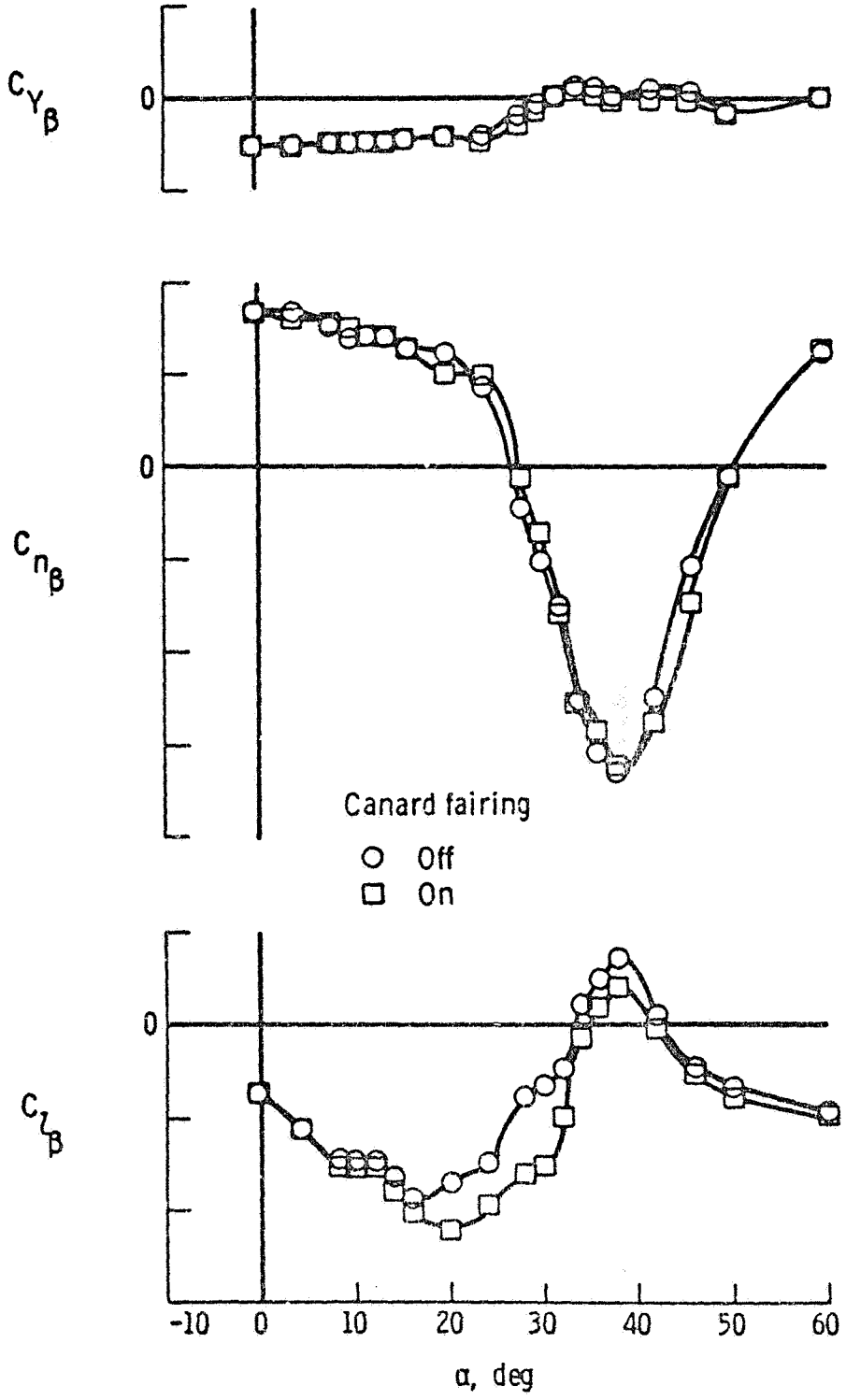

Figure 24. Effect of canard fairing on lateral-directional characteristics.

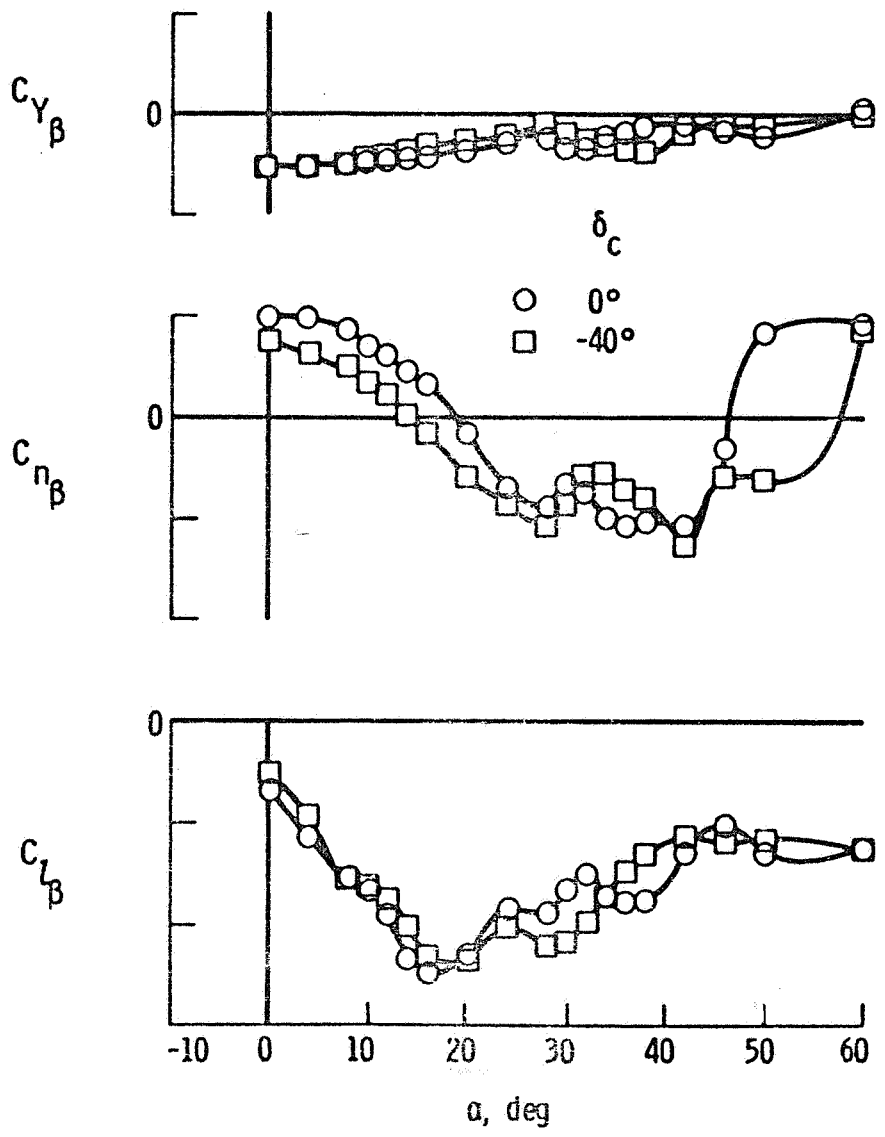

Figure 25. Effect of canard deflection on lateral-directional characteristics.

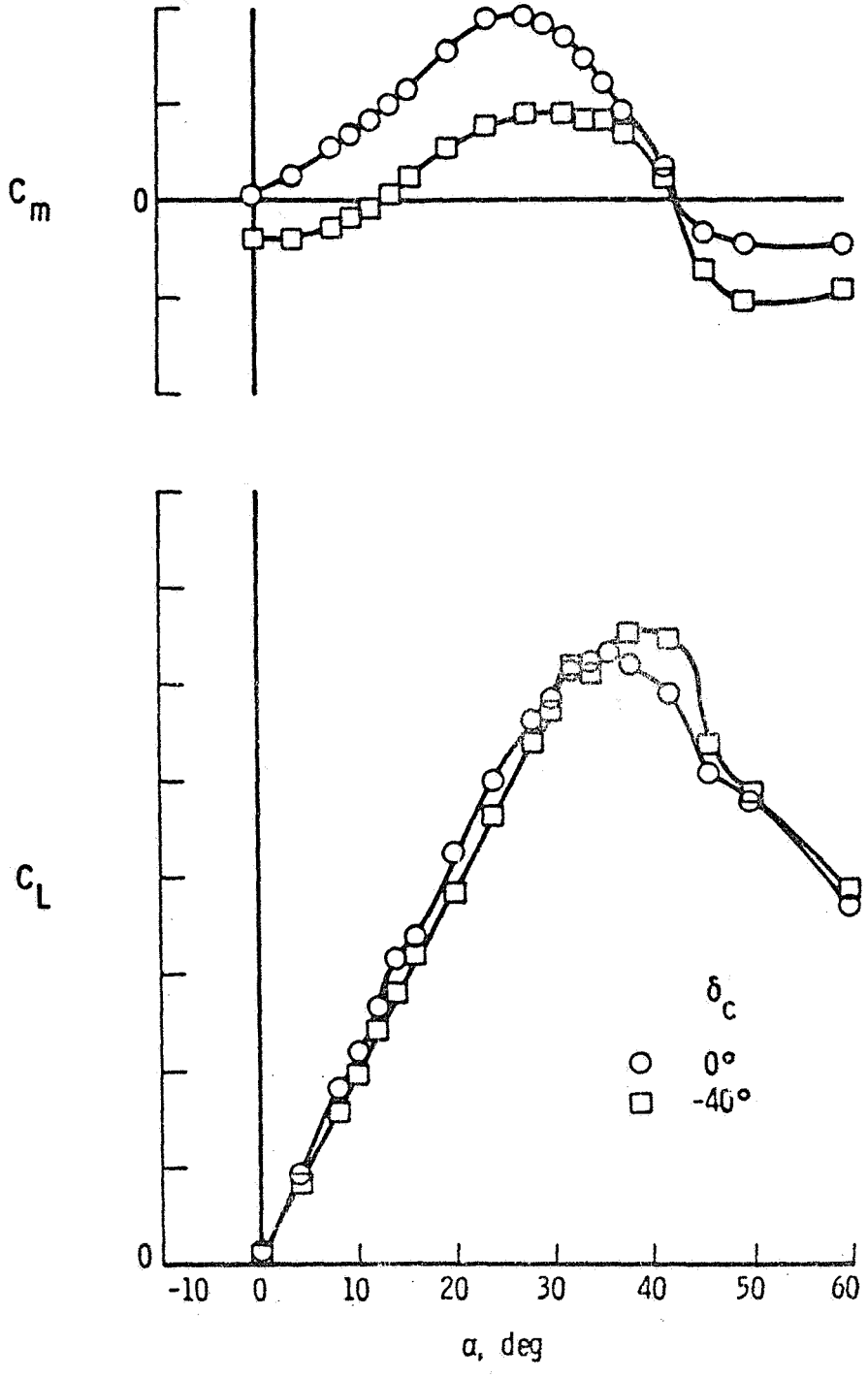

Figure 26. Canard effectiveness.

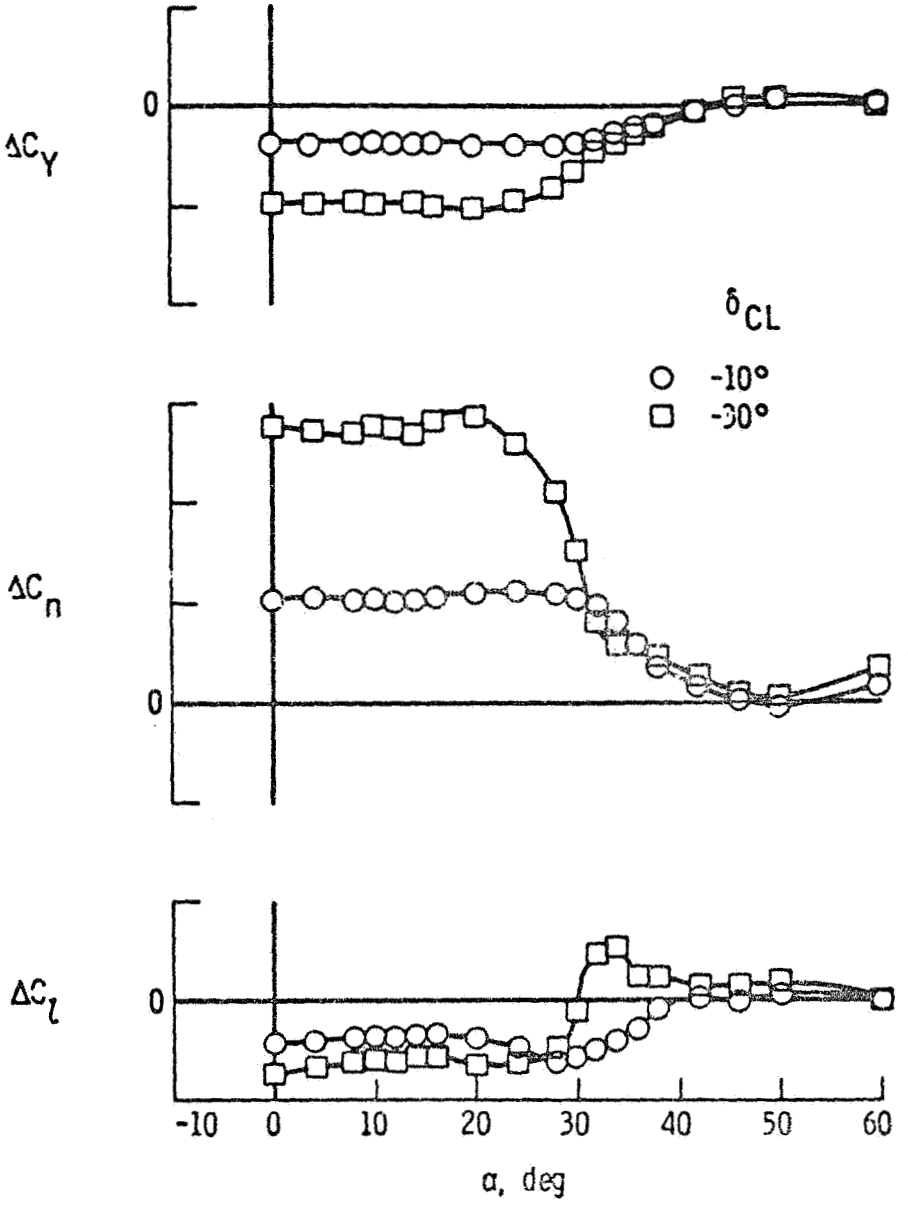

Figure 27. Centerline vertical tail effectiveness.

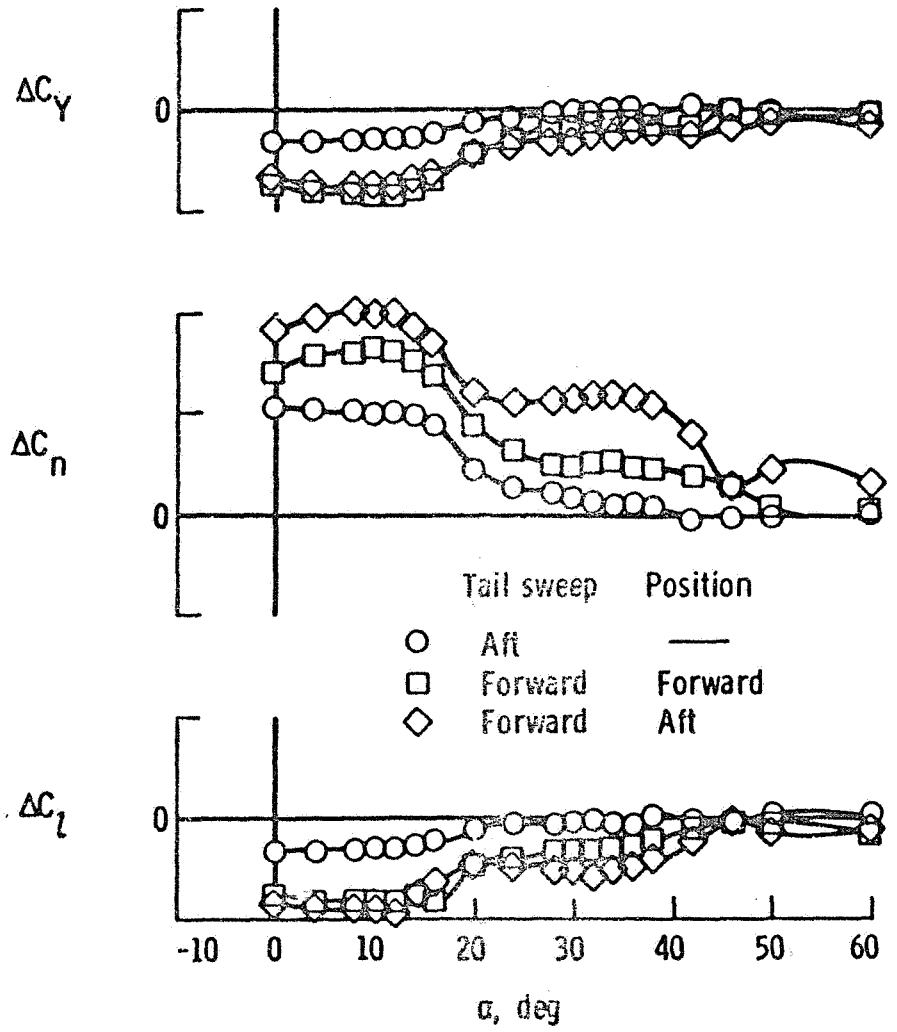

Figure 28. Effect of rudder hingeline sweep on rudder effectiveness. $\delta_r = -30°$.

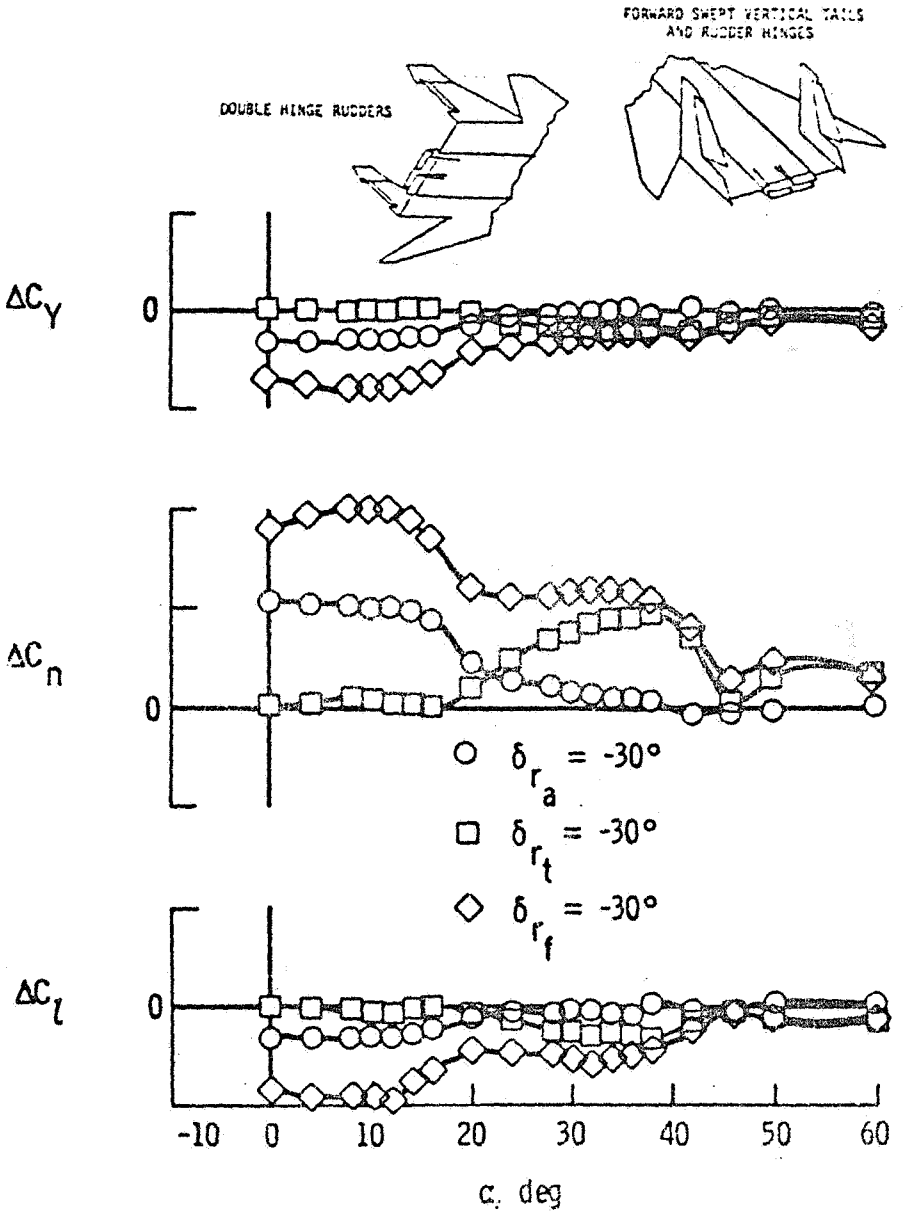

Figure 29. Tip rudder effectiveneses.

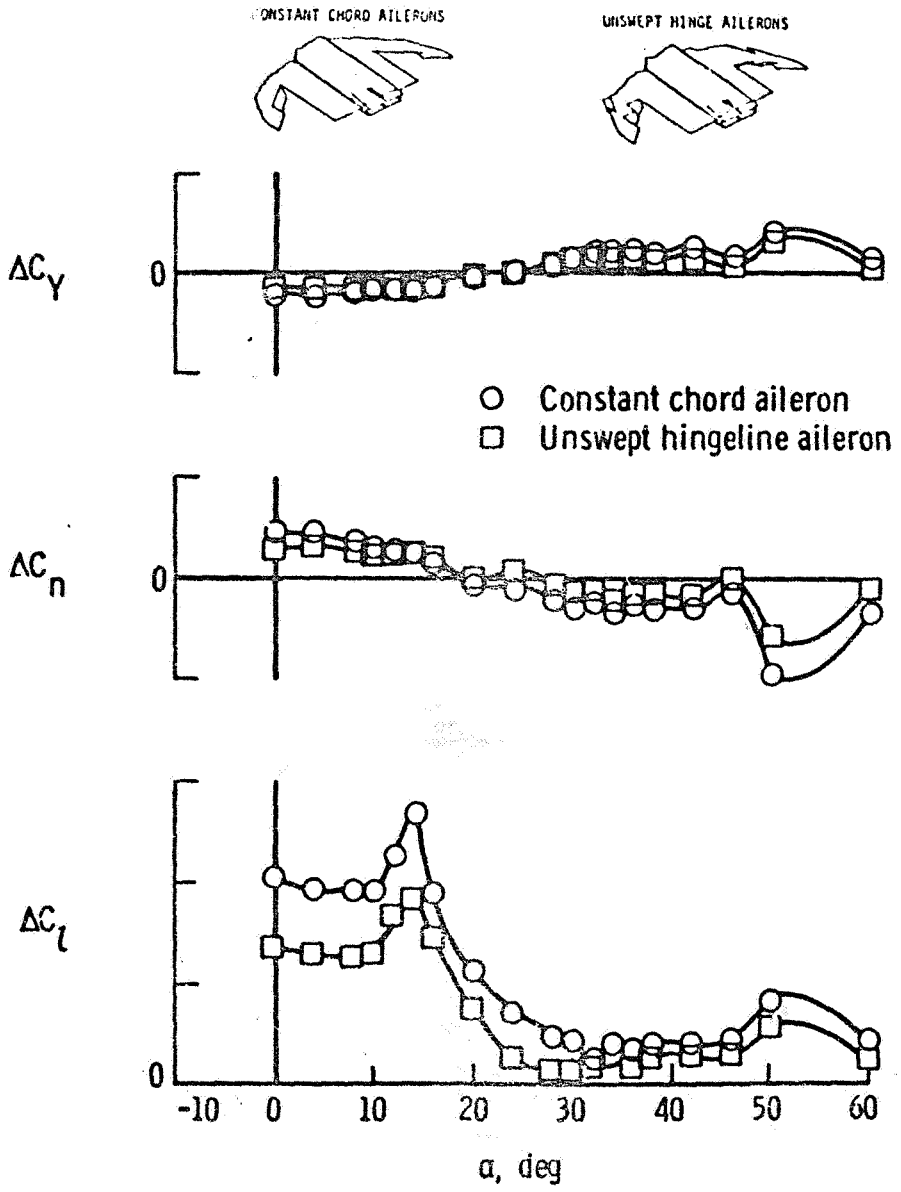

Figure 30. Effect of aileron geometry on roll control. δ_a = -20°.

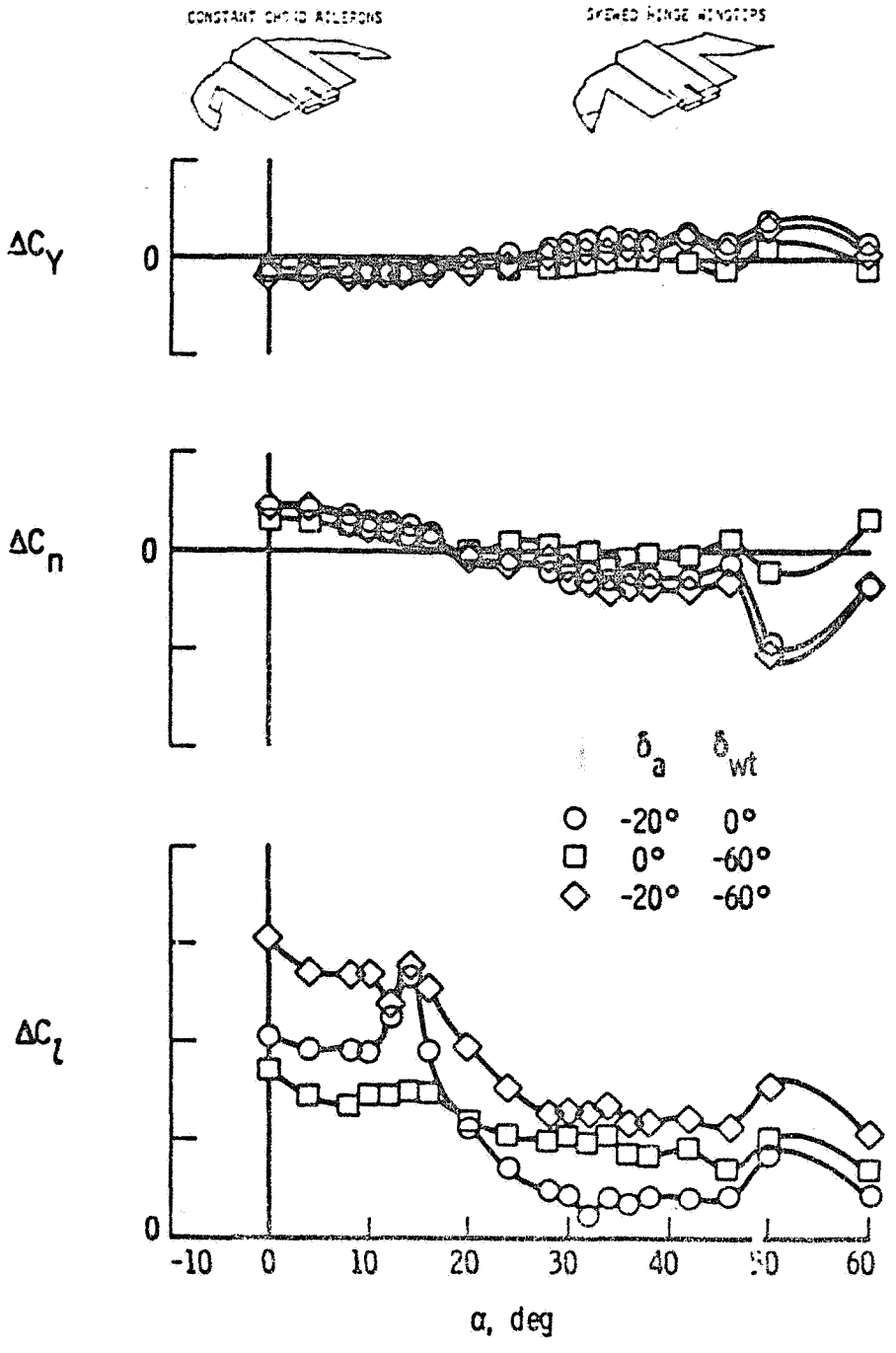

Figure 31. Effectiveness of wing tip deflection for roll control.

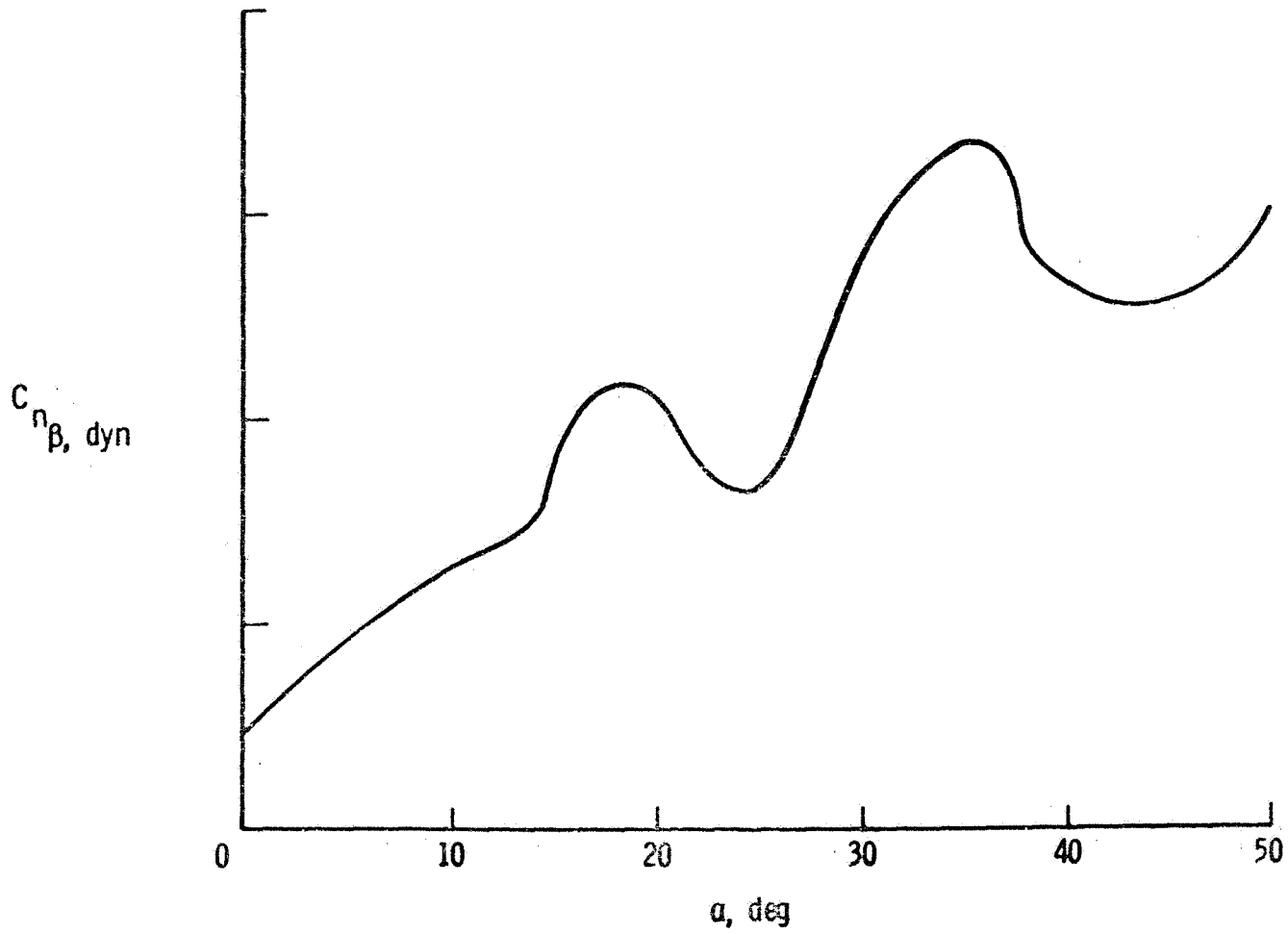

Figure 32. Departure resistance of test configuration.

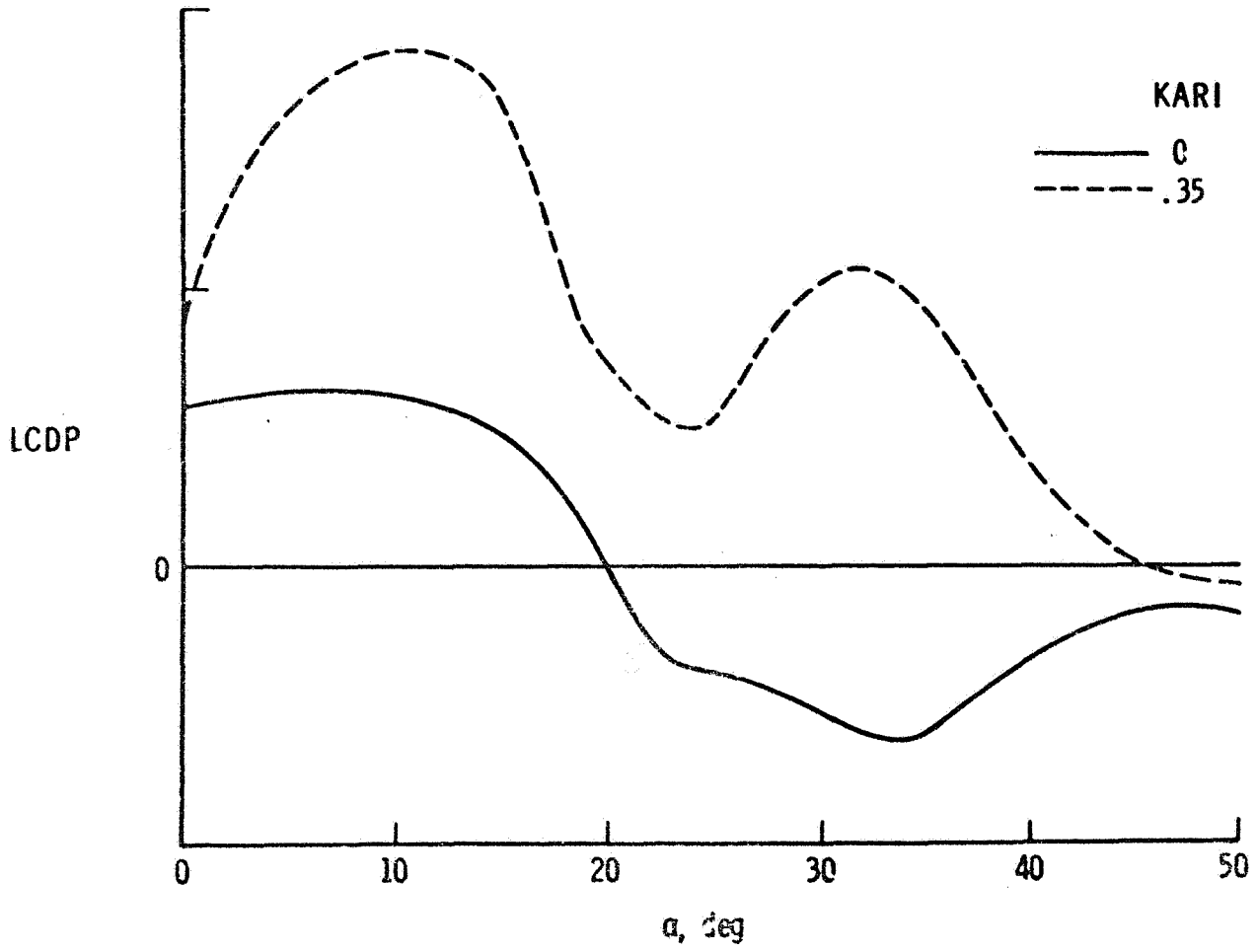

Figure 33. Effect of ARI gain on control response.

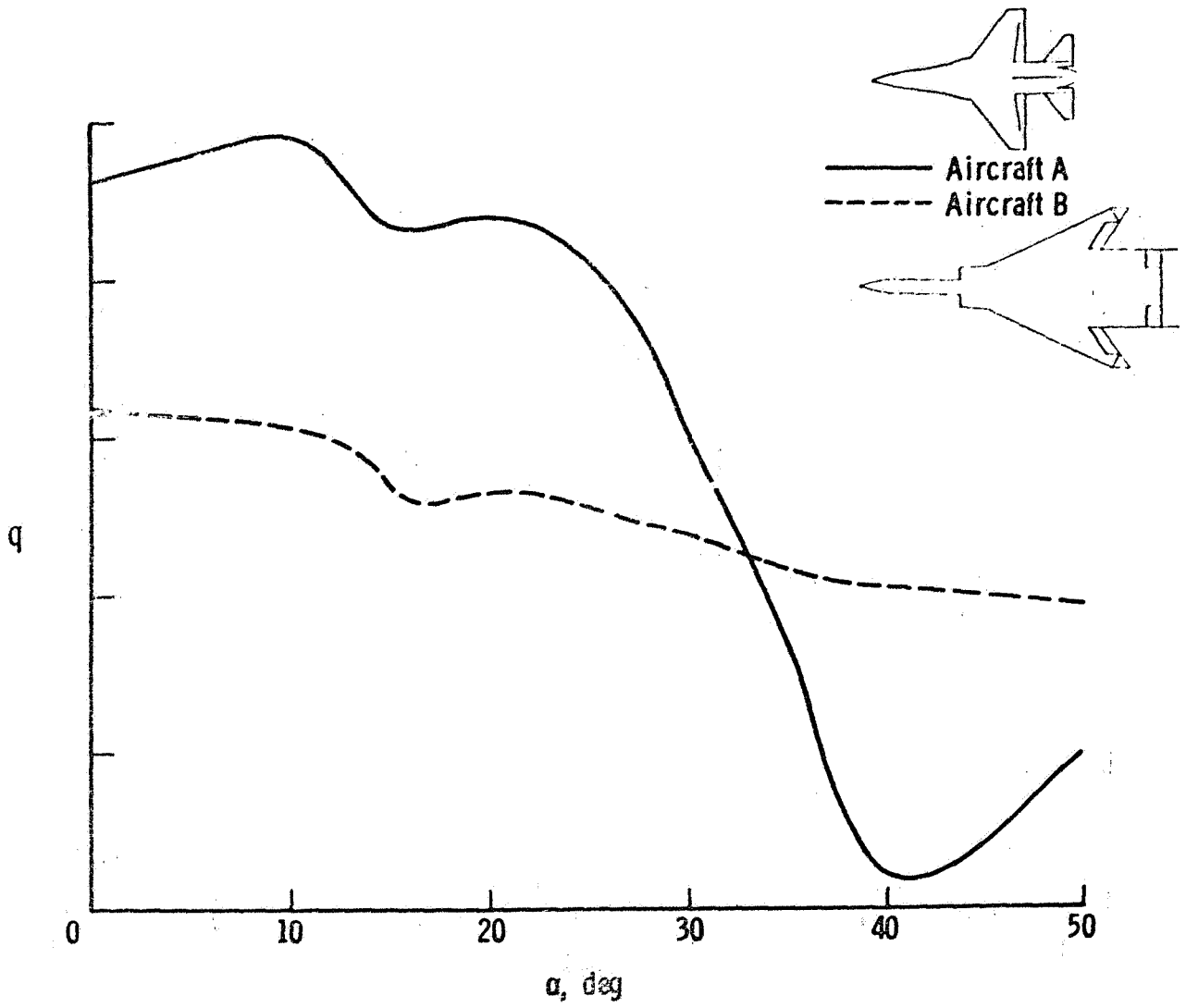

a. Pitch rate acceleration

Figure 34. Maneuverability comparison to current aircraft.

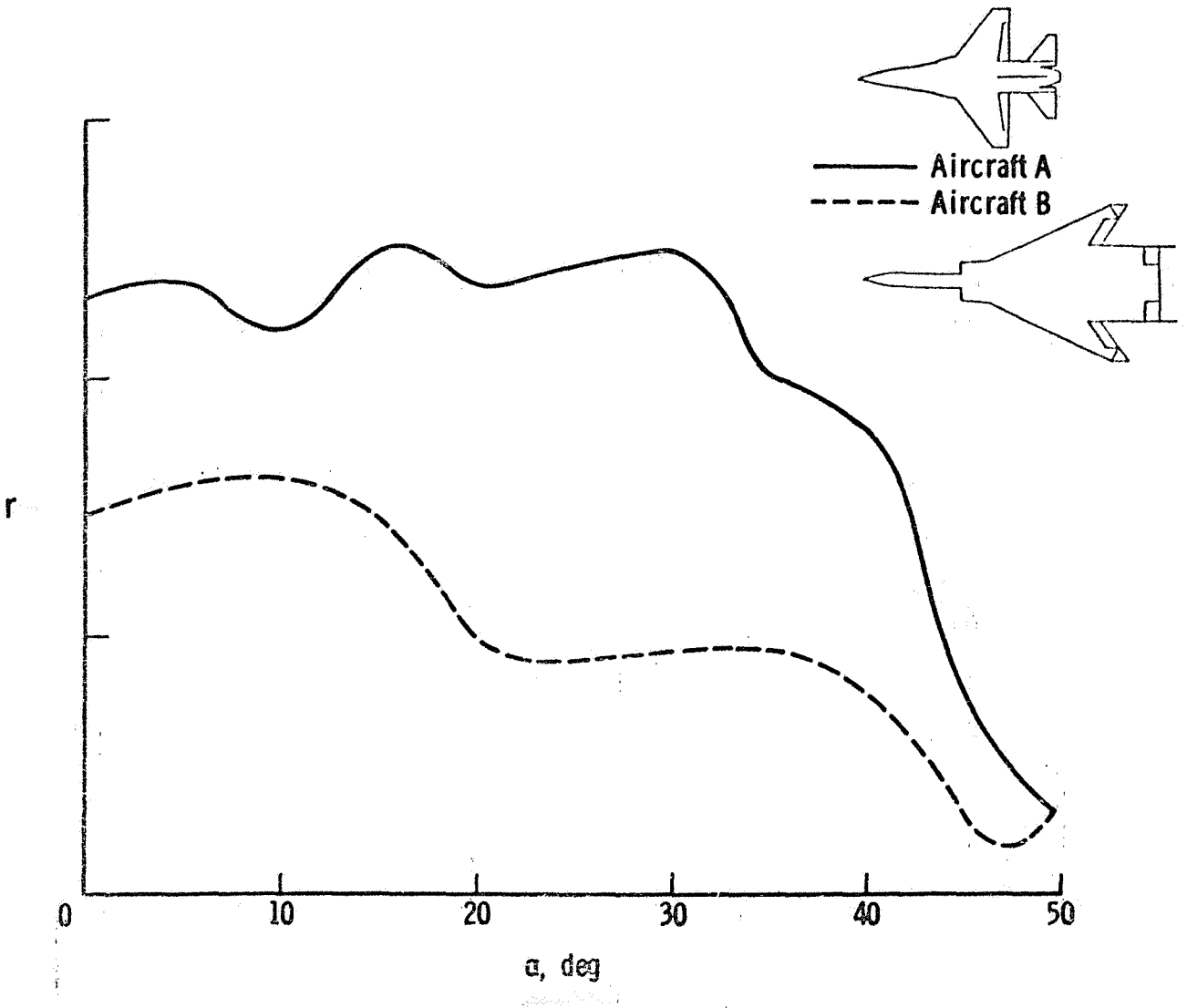

b. Yaw rate acceleration

Figure 34.- Continued

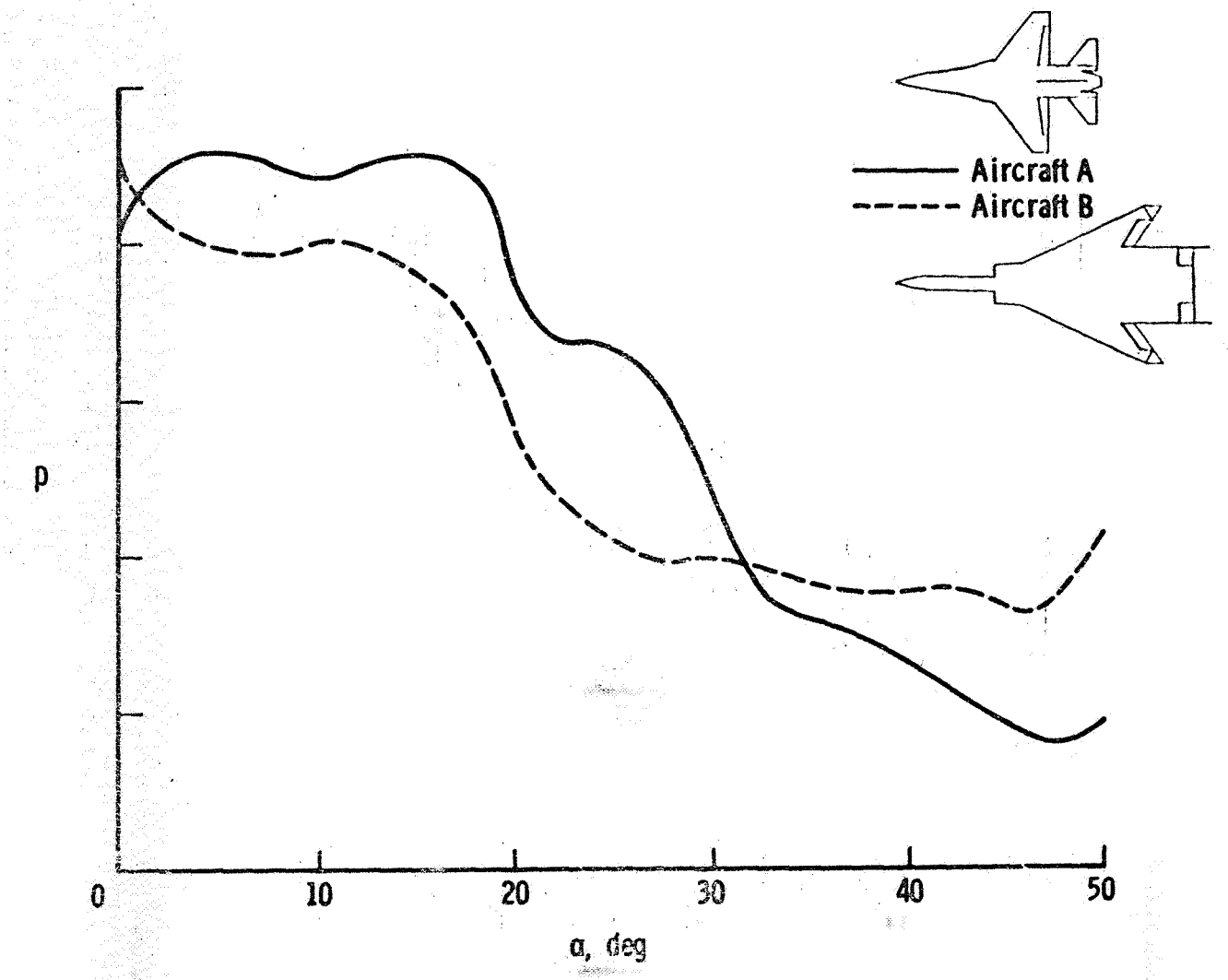

c. Roll rate acceleration

Figure 34.- Concluded

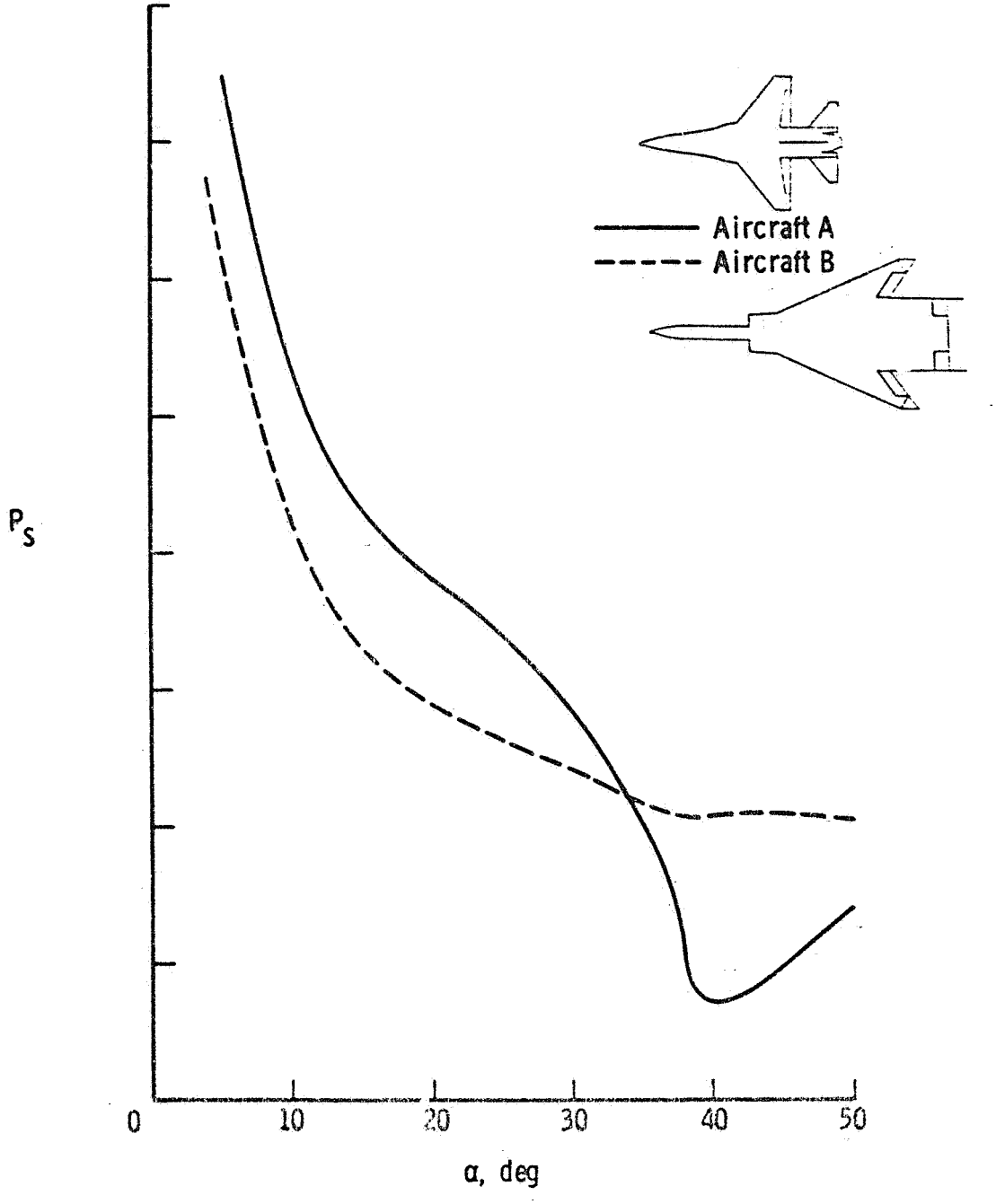

Figure 35. Effect of inertia coupling on maximum roll rate.